University of Nevada, Reno

A Mathematical Framework for Analysis and Design of Magnetic Climbing Mobile Robots

A thesis submitted in partial fulfillment of the
requirements for the degree of Master of Science in
Computer Science and Engineering

by

Cadence Motley

Dr. Hung M. La - Thesis Advisor
May 2021

THE GRADUATE SCHOOL

We recommend that the thesis
prepared under our supervision by

CADENCE MOTLEY

entitled

A Mathematical Framework for Analysis and Design of Magnetic Climbing Mobile Robots

be accepted in partial fulfillment of the
requirements for the degree of

MASTER OF SCIENCE

Hung M. La, Ph.D.
Advisor

Sushil Louis, Ph.D.
Committee Member

Gokhan Pekcan, Ph.D
Graduate School Representative

David W. Zeh, Ph.D., Dean
Graduate School

May, 2021

Abstract

Robotic platforms that can successfully traverse atypical environments like those found on steel bridges, turbines, and silos are currently being researched and developed globally through funding from a range of governments. Improvements to robots of this type are highly desirable because efficient and detailed inspection of infrastructure is in demand as the world's current infrastructure ages. In this thesis we propose a framework of analysis for the engineering and design of magnetic steel climbing mobile robots to standardize the industries approach toward these robotic solutions. This framework equips members of the computer science and engineering field with the knowledge to analyze their own design concepts and optimize for desired parameters. In addition, this framework provides engineers with the ability to quantify the degree of confidence they would prefer through the definition of factor of safety (FOS) equations. The application of this framework has assisted the design of two state-of-the-art robots created by the Advanced Robotics and Automation (ARA) Lab of the University of Nevada, Reno (UNR) and has also been used to analyze previous robotic designs. The ARA Lab's V3 and V4 robots designed through the application of this framework have been created. The successful functioning of them shows that the framework proposed in this thesis can efficiently predict operating capabilities and consequently, will help to reduce the frequency and cost of potential future project design failures by allowing designers to catch them before purchasing, manufacturing and physical verification testing is performed.

Acknowledgments

I would like to thank my advisor, Dr. Hung La, who funded my research and gave me the opportunity to pursue my passion for the creation of robotic systems. His guidance and recommendations have been instrumental throughout my degree. I would also like it to be known that his courses are the best. Next, I would like to thank Dr. Daichi Fujioka who I have spent these last few years working beside in teaching the university's mechanical engineering capstone students as a TA. My work with him has helped me attune my teaching abilities and helped take the edge of my oftentimes harsh coursework feedback while still keeping the standards of the course high. Without Dr. La and Dr. Fujioka, I would not have been able to pursue a masters degree, or have learned so much about research and teaching.

I would like to thank Brian Nagy from the mechanical engineering department for design and manufacturing discussion and help when I needed it. I would never have had the opportunity to become a machinist if he did not hire me back in 2018 and was not so willing to share his knowledge and skill with me. Without him, I would not have met Dr. La and would not have had the opportunity to pursue a graduate education. The skills he has taught me will undoubtedly continue to benefit me throughout my entire career. I am thankful for the tremendous impact that he has had in my life and will continue to have.

I would also like to thank my committee members Dr. Sushil Louis and Dr. Gokan Pekan for their advice and for taking the time to review the contents of my thesis.

Finally, I would like to thank the people in my personal life like my mother for being as supportive as she is and helping me when I needed it most. Chris Geiser for our discussions about philosophy, engineering and passions. Ashutosh Singandhupe for companionship among graduate students, guidance and reassurance when I was not feeling confident as a graduate student within computer science and engineering.

Finally, I would like to thank Habib Ahmed for our discussions in the lab and being a friend to talk to during short breaks.

I am fortunate to have the company of such wonderful people in my life, my success is in part due to the influence and impact of these people. Thank you!

This work is supported by the U.S. National Science Foundation (NSF) under grants NSF-CAREER: 1846513 and NSF-PFI-TT: 1919127, and the U.S. Department of Transportation, Office of the Assistant Secretary for Research and Technology (USDOT/OST-R) under Grant No. 69A3551747126 through INSPIRE University Transportation Center.

The views, opinions, findings and conclusions reflected in this thesis are solely those of the authors and do not represent the official policy or position of the NSF and USDOT/OST-R.

Table of Contents

List of Figures

Chapter 1

Introduction

1.1 Problem Statement

Steel bridge inspection is a dangerous job which requires in depth training on safe practices and knowledge about overall bridge and steel condition assessment. This job often requires people to enter very tight spaces between members or hang beneath the bridge. As a result, performing a steel bridge inspection can be extremely dangerous and costly. Work is being done to create robotics which can assist inspectors to dramatically improve the safety of conducting steel bridge inspections however the design process is often long, costly and does not always produce as substantial of results as initially intended. These works require an extensive and detailed set of analyses to ensure that a given design will function as intended. Through the application of the generalized framework for analysis of mobile climbing robots proposed in this thesis, future designers can reduce the time and cost of bringing a design of their own to its final stage of production by equipping designers with the abilities to critically check and analyze their own designs and through use of the Factor of Safety

(FOS) equations proposed in this paper.

1.1.1 Literature Review

Many recent works in the field of computer science and engineering have been aiming to create mobile robotics for a plethora of applications including inspection, exploration, repair, transportation of goods, manufacturing, warehouse management and even education and entertainment. Oftentimes these mobile robots mimic and take advantage of our knowledge in fields we already have a great deal of research in such as the automotive, military or aircraft industries benefiting car-like [10, 11], bicycle-like [12], tank-like robots [13, 14] and drones [15].

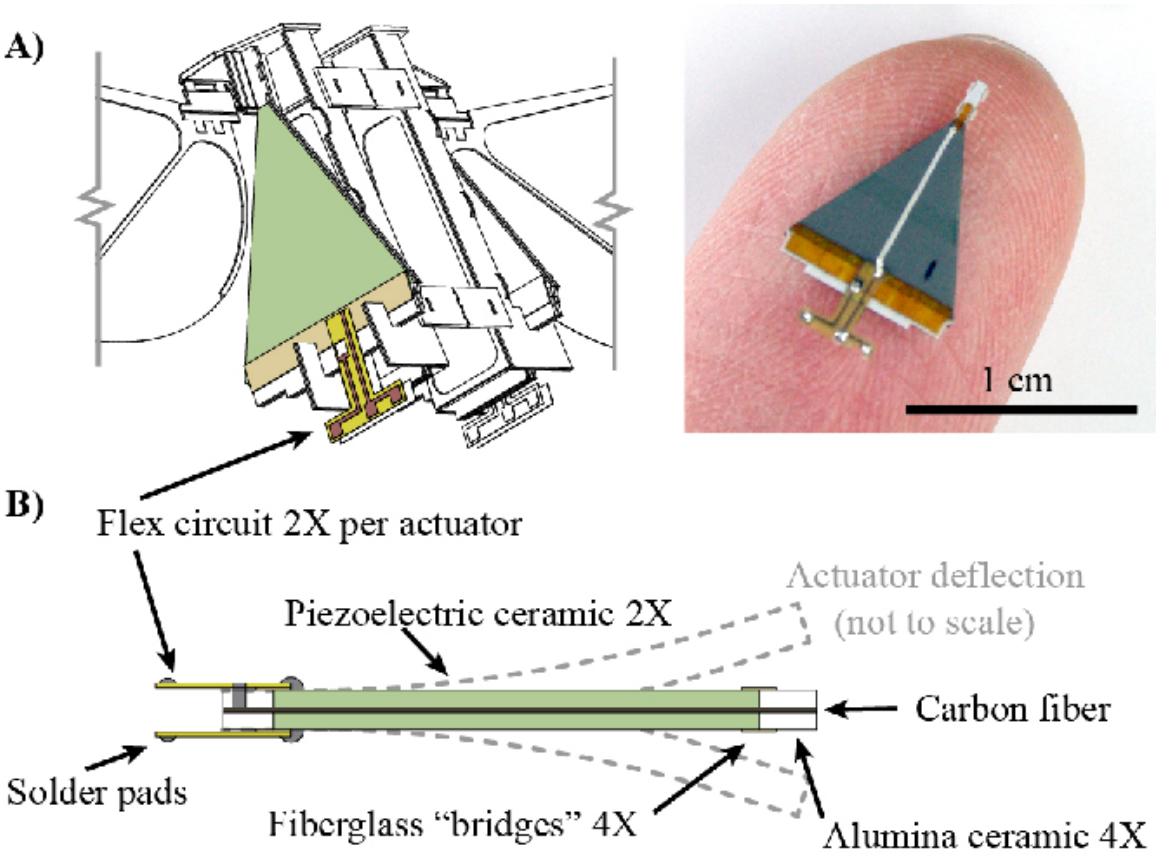

Figure 1.1: Robot smaller than the size of a fingertip. [1]

However, applications for mobile robots often extend beyond the environments

which we are familiar with such as robots which operate at the scale of insects [16,17]. These robots face environments at a scale very different from the one people experience in everyday life shown in Fig. (1.1). Challenges arise with the need to design around a systems natural frequencies and creating a system that can support the transportation of a payload [1].

In general robots which feature designs based in biomimicry [18] also feature their own unique challenges since these robots often utilize locomotion techniques which are unique to a particular species or tree of organisms. One work, aimed to recreate the flying capabilities of a butterfly [19]. Another, the swimming capabilities of fish [20], the designers had to create a robot capable of swimming in aquatic environments and controlling its buoyancy. These robots make use of locomotion techniques which are different from the methods we have used in the past. As a result, there is often a dearth of prior knowledge and past analysis and design to work from. This causes designers to have to create their designs from scratch without much to go on outside of observing the physical animal.

In the case of climbing robots, there are a variety of approaches that are commonly taken ranging from the application of dry adhesives [21, 22], suction cups [23] and magnets.

Here at the ARA Lab at the University of Nevada, Reno we focus on the creation of robots for the purpose of bridge inspection [24–32]. These robots climb through the use of permanent magnets on steel surfaces frequently found around steel bridges. Previous work performed testing on the bridge from the road [14,30,33–38]. However, recently we have begun to create climbing robots meant to traverse the underside of bridges which are not nearly as consistent as the environment commonly found on roadways. Bridges often have jutting edges and corners, round curving members, thin obstructions like cables, dirty surfaces which can be slick and oily or wet, gaps and

tight spaces that are inaccessible to people.

In the United States, there are 175,825 bridges containing major steel components [39]. In a recent report put out by the American Society of Civil Engineers in 2016, they found that "9.1% of the nation's bridges were structurally deficient" [40]. Part of this can be attributed to America's aging infrastructure and has potential for far reaching consequences should an unexpected bridge failure occur since America's roadways are a the backbone of our economy.

Figure 1.2: I-35W Bridge before and after collapsing [2, 3]

In 2007 the I-35W bridge over the Mississippi river in Minnesota collapsed unexpectedly resulting in the death of 13 people and the injury of another 145 [41]. In addition to the injury and loss of life, the economic impact was estimated to be a net loss of $120,000 per day by the Minnesota Truckers Association [42]. Work should be done to improve the safety, detail and efficiency of steel bridge inspections to mitigate the increased risk of collapses. There are a variety of recent works within the steel inspection robotics field. Some of these take surface based approaches and others take aerial ones. We will focus on surface based solutions since our robot [30, 34, 36–38] is a surface based solution as well.

CROC [4] and the hybrid climbing robot (V3) [43] feature the ability to move

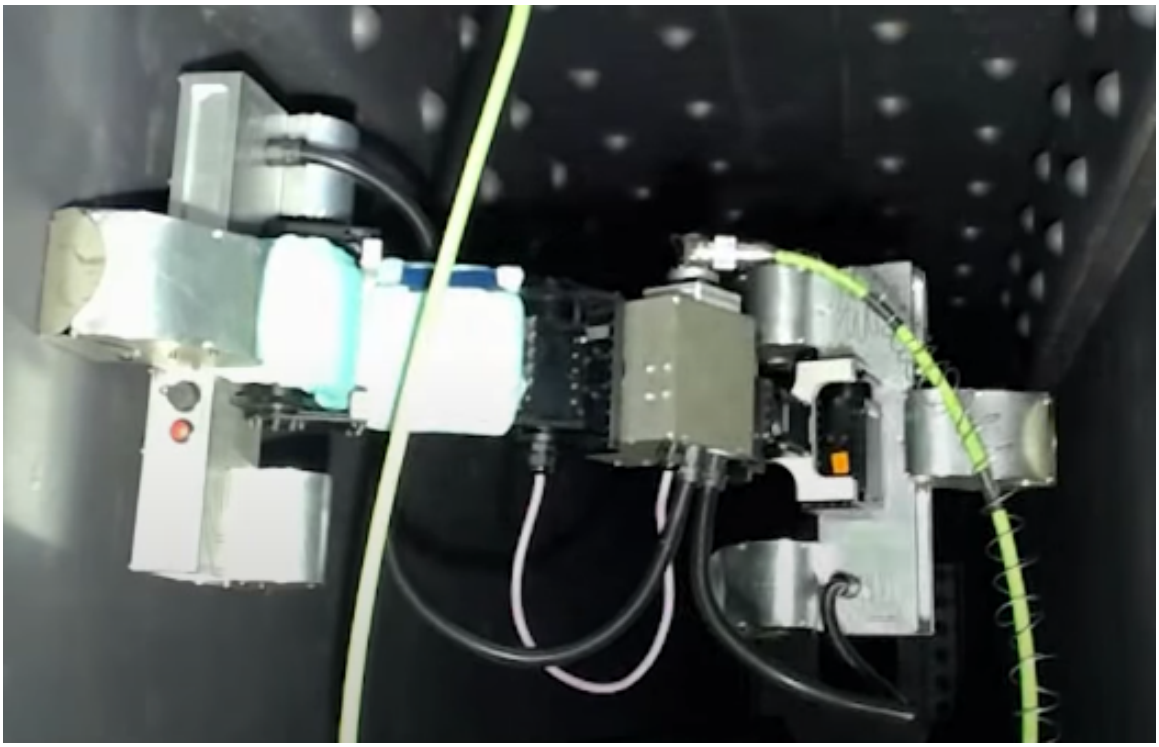

Figure 1.3: Picture of CROC Robot. [4]

around like an inch worm. While these robots have a great potential to move around and adhere to a very wide variety of areas, these robots suffer from being very complicated. The control frameworks needed to efficiently utilize these robots are computationally expensive and can require a lot of power. This is particularly disadvantageous since operation of these robots occurs in hard to reach areas on steel bridges where power is not as accessible as it would be in other areas.

MINOAS [44] and BIREM [5, 45] are smaller steel inspection robots. They both work for their intended purpose but cannot bear additional weight to do anything more than gather visual data. When inspecting steel, surface level data is not enough to properly provide a good quality inspection of a section of steel. This means that these robots do not eliminate the need for inspectors to physically go to the hard-to-reach areas that they may need to explore.

Another recent work by Helical Robots created a robot for inspection of wind

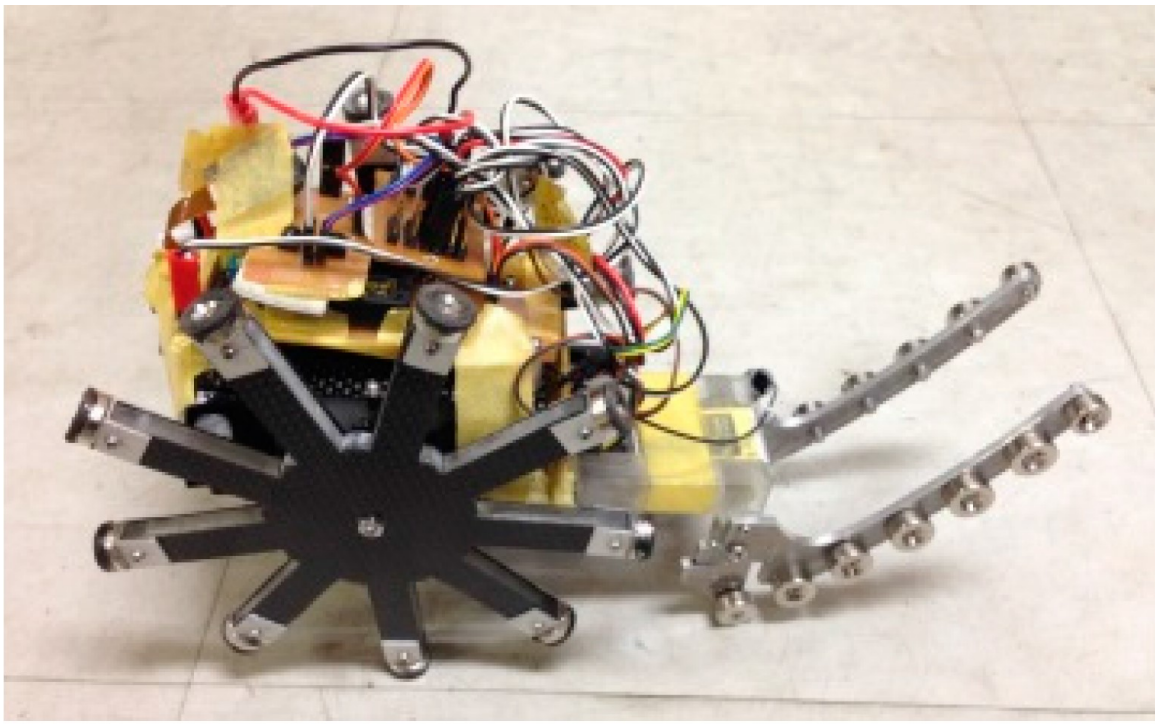

Figure 1.4: Picture of BIREM Robot. [5]

turbine towers [46] shown in Fig. (1.5). However, the robot is unable to transfer from the tower to the generator or to still blades because it generates its magnetic adhesion force at its center. This causes the robot to be unable to transfer between surfaces.

In general, steel climbing robots function in an environment which poses a unique set of difficulties and challenges to the robots functioning. These challenges include the need to travel over gaps, internal and external edges, over nuts and around cables and need to be able to function in unusual orientations including vertically and upside down. In our efforts to make these robots we noted a lack of established precedent and previous work that made an attempt to standardize an approach toward the creation of steel climbing robots. Therefore, after two years of research in this field and the analysis and design of a few robots, we propose a mathematical framework for the analysis and design of climbing mobile robots.

Figure 1.5: Helical robotics robot on wind turbine tower [6]

1.2 Surface Level Information

A great deal of the information that we will be discussing and building up from to create the analysis framework posed by this thesis is dependent on some prior knowledge and understanding of a few basic mechanical principals. This section will provide some of that information so that readers coming from a computer science and engineering background can better understand the framework and how to apply it to their own applications for the purpose of designing robots.

1.2.1 Forces, Moments and Torque

To start, all readers should be keenly familiar with Newtons second and third laws. The seconds states that $F = ma$. What this means is that a force acting on something

can be solved for if we know the mass and the acceleration of that object. Forces are in the unit of Newtons (N), mass in this paper will be referred to in kilograms (kg) and accelerations are in meters per second squared ($\frac{m}{s^2}$). One very common example of a source of acceleration is gravity pulling everything down (toward the center of the earth) at $9.81\frac{m}{s^2}$. Newtons second law tells us that a N (Newton) will therefore have units of $\frac{kgm}{s^2}$.

When discussing the forces acting on a body, we often define points at which we say that these forces are occurring and will draw an arrow to represent that forces direction as can be seen in Fig. (1.6). Forces acting on a body or point can be summed $\sum_{F_1}^{F_n}$ to determine the net force acting on that body. When doing this, forces acting in opposing directions will cancel each other out. Finally, if a body is in contact with an object or surface that does not move (is fixed), we often use a lined notation to note that it is not moving.Newtons third law states that forces are equal and opposite when acting between two objects for instance, if you place your fist on the desk and push down, your desk will also push back your fist. In slightly more complicated systems, we often refer to these forces as the reactionary forces in static analyses.

Moments are a bit of an extension of forces. The generic equation for a moment is $M = Fd$. Moments refer to the twisting/rotating effect created by forces that are exerted away from a stationary point, they have the units of Nm. The major thing to note about moments is that they are created by multiplying a force with a perpendicular distance and that the moment created can be in either a clockwise (CW) or counter clockwise (CCW) direction. The difference between a moment and a torque is that moments occur during static analyses and torques occur during dynamic analysis. Oftentimes, torques will refer to the output of an acting component such as a servo or a motor. Whereas a moment will occur at an instant (moment), a moment may not continue to exist in the next moment whereas torque will continue to persist

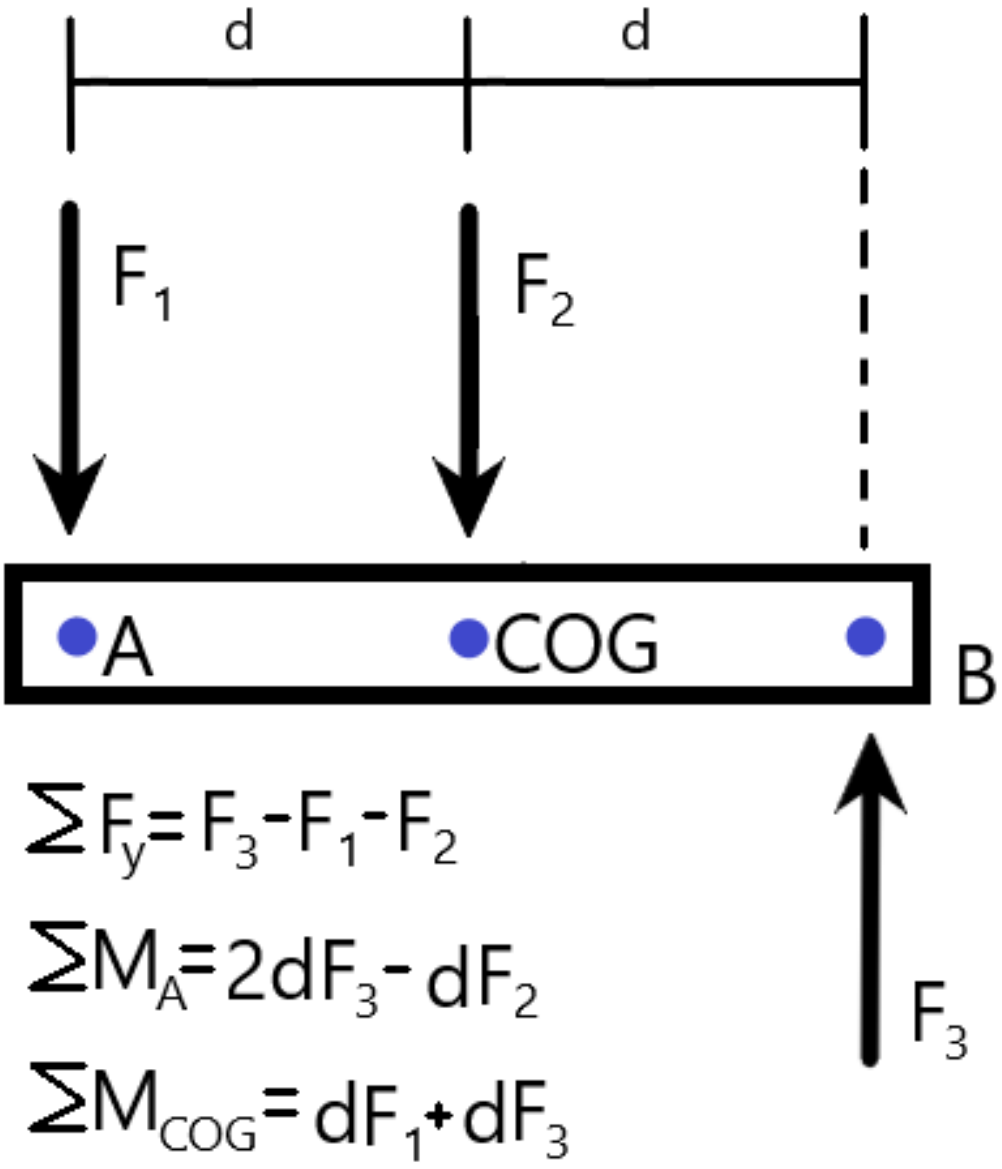

Figure 1.6: Example to build an understanding of Forces and Moments.

through movement of the body under consideration. A summation of moments or torques is always done about the particular point at which the rotation will to occur.

1.2.2 Statics/Dynamics

Within mechanical engineering there are two major branches of physical analysis types being static and dynamic. If an analysis is static, we are making the assumption that the objects being analyzed are not moving and are in static equilibrium creating a set of reaction forces. These assumptions require that the sum of forces in each direction are zero and that the sum of moments is also equal to zero ($\sum_{i=1}^{n} F_i = 0$, $\sum_{i=1}^{n} M_i = 0$). Dynamic analyses on the other hand do not make this assumption and instead allow for the object under analysis to potentially move between instances of time. Dynamic systems are not assumed to be at static equilibrium.

We often use static analyses to solve for the point at which these assumptions fall apart since they will tell us the limit of our systems. In the case of analysis of structural members, static analyses can mathematically tell us under what conditions the object will fail by breaking. These allow us to solve for the maximum payload of the system is before it will fail in which our static assumptions will fall apart and the system will begin to move.

Dynamic analyses allow us to determine the behavior of our system when it is moving and can be used to determine how much torque or force we will need to maintain movement that we do want. They can also give us information about the forces that will be created in our system based on how movements are performed in the system. For instance, if you grab an object of a few grams and fully extend your arm. Now, trying to move that object up and down in sharp quick movements, now try the same motion but with slower and smoother movements. These are the forces we can calculate using dynamic analyses; we can use this information to inform our decisions on how to move to reduce the effect of unwanted forces and maximize those of wanted ones.

1.2.3 Loads, Stresses and the Stress-Strain Curve

When we discuss a load, we are referring to something which is creating a force in our system. The source of this load could be from a myriad of things however in the context of this paper, loads will be created as a result of the accelerations of mass. This primarily is from gravity however in some instances it can be created from the magnetic field of a permanent magnet, or due to the acceleration induced in parts of a robot from the actuation of a joint.

Stresses (σ) are forces applied over an area. The equation for a generic stress is $\sigma = \frac{F}{A}$ where A is the area the force is acting on. Stresses have a unit called pascals Pa with base units of $\frac{N}{m^2}$. Oftentimes, we write stresses in larger units to reduce the number of significant figures; megapascals (MPa, $\frac{N}{mm^2}$) or gigapascals (GPa, $\frac{kN}{mm^2}$)

Strain is the elongation of a material under stress. The generic equation for it is $\epsilon = \frac{\Delta L}{L}$. When a material is under stress, it tends to elongate and the equation for it is the ratio between that objects elongated length divided by its original length before the application of its stress. A classic everyday example of this is in the plastic bags given out at grocery stores, when pulled these bags typically tend to elongate considerably before breaking.

When considering the benefits of using a material or comparing them for structural components, we often compare each of those materials stress strain curves, density and chemical properties. The stress strain curve describes how a material responds under stress by showing the behavior we can expect from that material under those conditions. The stress strain curve of a material gives us information about that materials elastic modulus (Young's), yield strength, ultimate strength and fracture strength. The y-axis is the measure of stress in the material and the x-axis is a measure of how that material is straining (elongating) as a result of the stress on it. The major takeaway from Fig. (1.7) is the distinction between the elastic and plastic

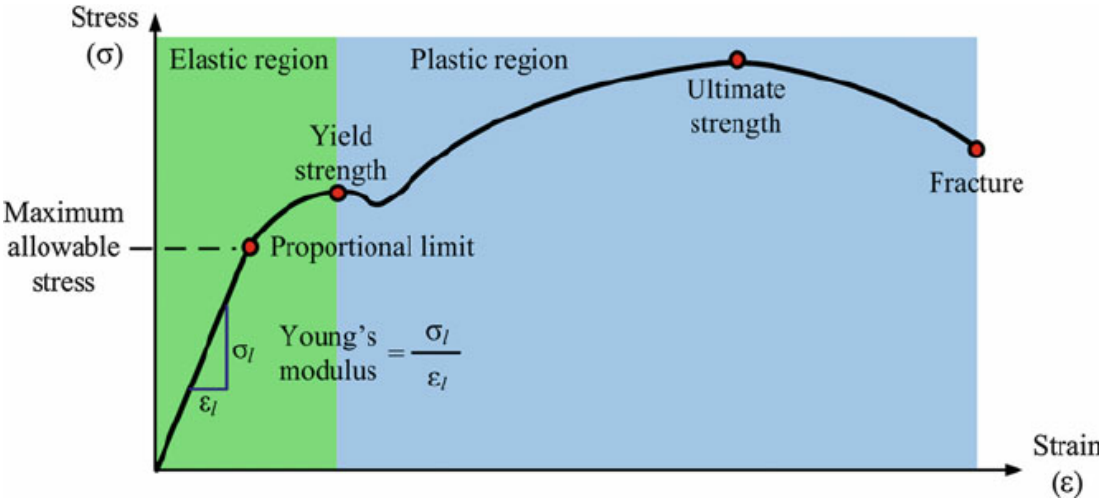

Figure 1.7: The Stress Strain Curve of a Ductile Material [7]

regions. When a material is in the elastic region it will go back to its original length (shape) based on the slope of the elastic modulus to the x-axis. What this means is that the given material can withstand up to its yield strength before it will begin to permanently elongate (deform). If a structural member experiences a stress higher than its yield strength then the part will be permanently changed and we can no assume that the system it is in will distribute and withstand stress in the same way that the system was designed.

All materials have their own stress strain curve and will respond differently to the stress on them based on their mechanical properties. For instance, steel is a strong metal whereas concrete is a strong ceramic. These change how the given material will respond to stresses in it. The ductility of steel makes it an excellent structural material in tension (pulling) but a poor material to utilize when in compression (pushing). The inverse is true for concrete as a brittle ceramic.

1.3 Contributions

In this thesis we create a mathematical framework for design and analysis of magnetic climbing mobile robots which can reduce the cost and time required to design and fabricate magnetic climbing robots. The framework provides an in-depth baseline of analysis for robots of this type and designers can use these analyses to design their system around desired parameters for optimization. Users of this framework can also know that their robot will function before making it through their ability to calculate their numerical confidence with the factor of safety equations.

Through the application of this framework, two state-of-the-art magnetic climbing robots have been successfully designed and created as shown in Figs. (3.11) and (3.3)

1.4 Thesis Organization

This thesis will first start with the static analyses by discuss how they are developed, how they can be applied to a design and defining some criteria (Factor of Safety, FOS) so that the designer can be confident their designed system will function as intended. Then, we will discuss the dynamic analyses doing the same thing. After this, we discuss the geometric requirements of a climbing system to pass internal and external edges to end chapter 2. After completing discussion of the framework of analysis, we discuss how the material described in the framework within chapter 2 has been applied to assist with the design and analysis of three of the ARA Labs robots in chapter 3. Chapter 4 will be the conclusion and future works section of this thesis.

Chapter 2

Mathematical Framework for General Analysis of Designs

This section of the thesis is particularly long, and interconnected. Be sure to take the time to understand each successive section as many sections draw from the conclusions and equations defined in previous sections. We start with Turn Over and Sliding Friction Analyses, discussing the Lead Screw and Wheel Steering Analyses, Finite Element Analyses (FEA), and finally the Contact Stress Analyses. Then, we will be discussing some of the expansion Analyses starting with Transformation Analyses next, the Impact Contact Stress Analyses, then a discussion of Robotic Maneuverability and finally, our Wheel Obstruction Analyses.

2.1 Base Analyses

2.1.1 Turn Over Analyses

A Turn Over Analysis is performed to determine a given robots ability to resist toppling over and off a steel surface at any point while operating. It is particularly central to the analysis of all climbing implementations of mobile robots since failure while in use from turning over would likely cause the complete destruction of the robot and its equipment.

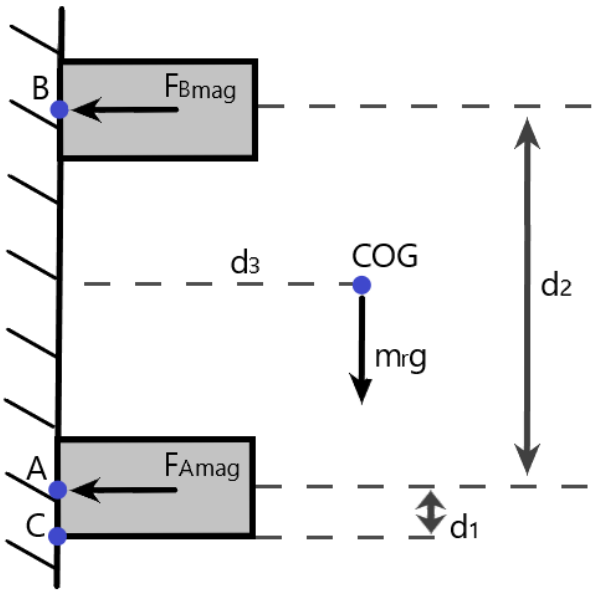

Figure 2.1: Generic Turn Over Diagram for a four Wheeled Robot (Front/Side View). The grey boxes represent wheels in contact with some fixed surface on the left at contact points A and B. The center of gravity (COG) is represented as a point mass.

d_1 is half the width of a wheel, d_2 is the distance between the wheel subsets contact points and d_3 is the height of the given robots center of gravity (COG) from the contact surface. m_r is the total mass of the robot, g is acceleration due to gravity, and F_{Amag} and F_{Bmag} are the forces exerted by the magnets toward the contact surface

(made of a ferrous material like carbon steel).

A turn over analysis should consider all orientations in which the given robot would be the most susceptible to this type of failure mechanic. This will typically result in two scenarios being considered when the robot is vertical or horizontal from a birds eye view of it. To start, we take a moment at point C in Fig. (2.1); the point at which turning over would occur.

$$M_C = d_1(2F_{Amag}) + (d_1 + d_2)(2F_{Bmag}) - d_3 m_r g. \tag{2.1}$$

In Equ. (2.1) we sum all moments generated by the forces acting on the given robot. In this case there are three terms, two created the the forces of the magnets and one created by the acceleration of the robots mass due to gravity. A robot would fail due to turning over when M_C is negative. Next, we write an equation to determine how much additional mass could be supported by the robot under the assumption that the COG is preserved.

$$m_e = \frac{M_C}{d_3 g}. \tag{2.2}$$

Equ. (2.2) is the equation for maximum equipment load (m_e). This equation tells the designer how much additional mass can be supported by the design. It is generated by setting M_C equal to the acceleration due to gravity term and solving for m_r which we substitute with m_e. Future worst case scenarios will include the m_e term with the m_r term by summing them ($m_r + m_e$). If M_C is negative then this equation will tell the designer how much mass needs to be removed from the robot to prevent failure.

$$FOS = \frac{m_e}{m_r + m_{equipped}}. \tag{2.3}$$

We define an equation for the factor of safety in Equ. (2.3) against turning over by dividing the maximum equipment load of the robot by the robots mass plus the actual additional mass equipped onto the robot ($m_{equipped}$). Generically a FOS is the ratio between a given things absolute potential and its required potential for the given scenario. Since failure of this type is particularly catastrophic, a high factor of safety $(3-5)$ is strongly recommended. Especially so to account for the potential shifting of the COG of the robot away from the contact surface as a result of added equipment for future research purposes.

2.1.2 Sliding Friction Analyses

A Sliding Friction Analysis is done to ensure that a robots design will generate the required friction to support its own weight when climbing [47]. This analysis is critical to a given robots ability to function but will not result in the complete loss of the robot and its equipment should failure occur. While the robot can be retrieved, the operation behind retrieval would be extremely dangerous, time consuming and costly.

A given robots angle will be represented by θ and will begin at the standard starting location on a unit circle with the robot facing to the right. This angle is important to consider in future analyses since gravity will effect the robot differently depending on how it is oriented on the surfaces it is traversing.

$$F_F = N\mu. \tag{2.4}$$

Equ. (2.4) is the generic equation for the force of friction (F_F) between two surfaces. We will need to determine the net normal force (N) and the friction coefficient (μ) acting between the two surfaces to calculate how much friction the wheels can generate with he surface they are on.

$$N = 2F_{Amag} + 2F_{Bmag} + (m_r + m_e)gcos(\theta). \tag{2.5}$$

To start, Equ. (2.5) is derived by summing all of the forces which act perpendicular to the surface the robot is adhered to to solve for the net normal force. We add the forces exerted by the magnetic wheels and the force generated due to the acceleration of gravity on the mass of the robots. Note how m_r now also has m_e added to it and the term is multiplied by the cosine of *theta* to account for the robots orientation. Next, we can setup an experiment to determine the coefficient of friction between SBR rubber and generic carbon steel.

Coefficient of Friction Determination

The friction coefficient between two materials can be solved for by setting up a small experiment in which both materials are put into contact with one another and a small mass pushing them together.

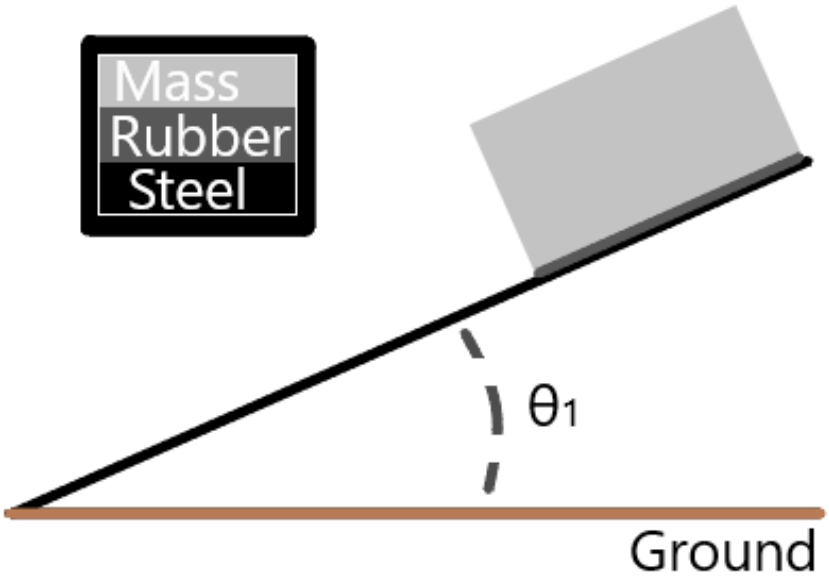

Figure 2.2: Friction factor test setup.

In our case, we used a block with the rubber coating adhered to one side and a steel beam as shown by Fig. (2.2). By raising one end of the steel beam and a device to measure the angle of the beam (θ_1) at a given instance relative to the ground. θ_1 can be determined when the block with the rubber coating on its face first begins to slide. The friction coefficient can be determined by taking the tangent of θ_1.

$$\mu = tan(\theta_1). \tag{2.6}$$

After 30 trials and with Equ. (2.6), we determined that $\theta_1 = 35^\circ$ and therefore that, $\mu = 0.7$ for contact between SBR rubber and generic carbon steel.

Sliding Friction Analyses

Once the friction coefficient and the normal force have been solved for we can derive and solve for the given robots friction with its contact surface.

$$F_F = N\mu - (m_r + m_e)g|sin(\theta)|. \tag{2.7}$$

Building on Equ. (2.4) by adding a term to account for the effect of the force of gravity (which acts against the robot) and multiplying it by the absolute value of the sine of the robots orientation at a given instance, we can write Equ. (2.7). This equation solves for how much force the designed robot will generate with a surface. If F_F is negative, the robot will fail to support its weight and will slide along the surface it is on.

$$m_e = \frac{N\mu}{g} - m_r, \quad for \quad \theta = 90^\circ. \tag{2.8}$$

$$m_e = \frac{2F_{Amag} + 2F_{Bmag}}{g} - m_r, \quad for \quad \theta = 180°. \tag{2.9}$$

The maximum equipment load that can be supported in this analysis type will not typically be the same as the Turn Over Analysis results since each analysis is effected by a myriad of different variables. Equs. (2.8 and 2.9) are created by setting $F_F = 0$ (The tipping point where not enough friction is generated and sliding will occur) and solving for m_e. Since each analysis type can vary widely depending on the designers choices, it is important to note that m_e should be thought of as an arbitrary amount of mass that we consider adding to the robot to allow us to calculate a given designs limits. The same FOS Equ. (2.3) may be used, values between 3 and 5 should be sufficient to ensure that failure does not occur.

2.1.3 Lead Screw/Wheel Steering Analyses

The Lead Screw and Wheel Steering Analyses performed were analysis to determine the required torque output from a given motor or servo to perform a desired action. For the lead screw, it was necessary to raise and lower a subassembly and for the wheel steering, we needed to rotate a wheel in order to give the robot the ability to steer its wheel. These analyses were important to ensure that the design would function as intended before purchasing.

Lead Screw Analyses

The purpose the Lead Screw Analysis is to determine how much torque is required to turn the lead screw which will result in the lifting of a subassembly. This analysis was part of our V3 robot analysis which had an array of small permanent magnets that it were apart of lower plate that the robot would raise and lower to change the

robots adhesion force with the surface it was on. Failure of this type would result in the robot being unable to lift the subassembly on the lead screws.

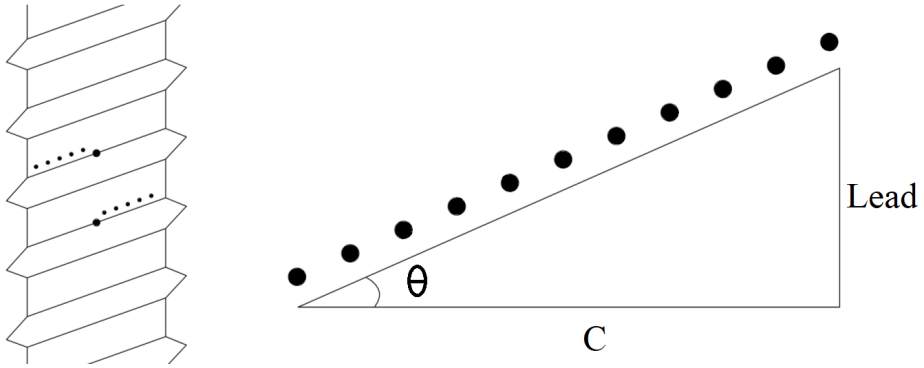

Figure 2.3: Lead screw 'unrolling' diagram.

To calculate how much torque would be required, we need to determine how much of the total adhering force from the magnets would translate into a moment in the lead screws.

$$\theta = tan^{-1}(\frac{Lead * 1rev}{2\pi C}). \tag{2.10}$$

Fig. (2.3) shows how we examine the lead screw to write Equ. (2.10). The equation effectively 'unrolls' the thread depicted in Fig. (2.3) to determine the angle at which a downward force would translate into creating a moment in the lead screws direction.

The variable (θ) represents the pitch of the thread on the lead screws, and k is the numbers of servo-lead screws acting. r_L is the radius of the lead screw, and m_{LA} is the mass of the lower assembly (subassembly) that is being lifted. n is the number of permanent magnets on the lower frame, and F_{mag} is the force one magnet creates. C is the circumference of the lead screw.

$$F_{LA} = \frac{nF_{mag} + m_{LA}g}{k}. \tag{2.11}$$

A summation of forces about the subassembly is done, yielding Equ. (2.11). There are two terms, one from the force of the permanent magnet array and the second from the acceleration due to gravity of the subassmebly. This is all then divided by k since the force will be distributed roughly equally between each of the designs lead screws.

$$M_{CR} = r_L F_{LA} tan\theta. \tag{2.12}$$

We now compute the moment the lead screws experience as a function of r_L, F_{LA}, and θ. Where the point CR is the center of the lead screw. This allows the designer to determine what servos would be needed to output the required torque to overcome the moment described from Equ. (2.12).

Wheel Steering Analyses

For a robot with the ability to steer a wheel, we need to analyze the torque required to turn the wheels in a given moment. Since static friction is greater than kinetic friction, we will be assuming that the robot is stationary when it turns its wheels. At any given instant, the wheels have a contact line with the surfaces they are on and a point at which the center of rotation (CR) occurs when steering. Our robots wheels have been designed to have a center of rotation at the center of the wheels width. This has been done to minimize the required output torque of our steering servos and to reduce steering complexity from the case of castor-like wheels. Failure of this type would result in the inability of the robot to steer its wheel.

A wheel steering analysis builds off of the sliding friction analysis of the given design's as shown in Fig. (2.4) where F_F on the right chart is divided by the number of wheels which is shown as 4 since our labs robots typically have 4 wheels. This is to represent the distribution of the friction generated by the robot in each wheel.

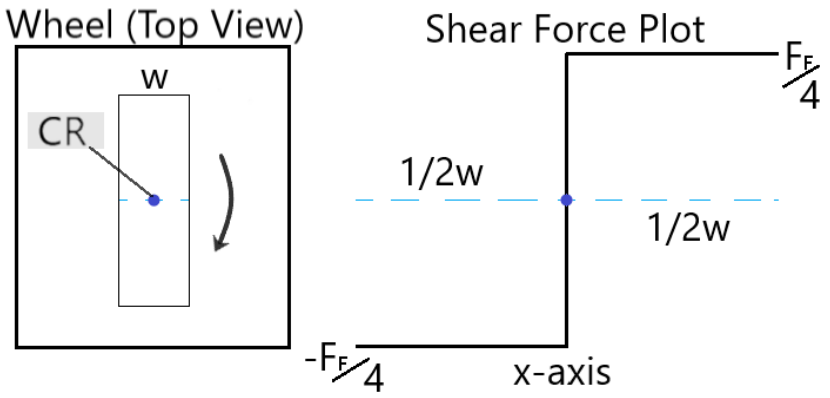

Figure 2.4: [left] A top down view of a wheel with width (w) which is rotating about point CR. [right] Shear force diagram along the wheels contact line.

$$M(x) = \int_a^b V(x)dx. \tag{2.13}$$

Drawing on insights from Euler-Bernoulli beam theory [48] on the relationships between shear forces and moments we can write Equ. (2.13). We create a shear force (V) diagram about the contact line as shown on the right side of Fig. (2.4) with a magnitude of $\frac{F_F}{4}$. Where x is distance along the contact line from the center of rotation.

$$V(x) = \frac{F_F}{4}. \tag{2.14}$$

The force of friction in Equ. (2.14) always acts in opposition to the rotation of the wheel and is a constant since the robot is stationary.

$$M_{CR} = \frac{F_F w}{4}. \tag{2.15}$$

We focus on half of one side of the shear plot because it is symmetrical and can write Equ. (2.14). We now plug Equ. (2.14) into Equ. (2.13) and integrate. Next we substitute $x = \frac{w}{2}$ and $M(x) = 2M_{CR}$ to get Equ. (2.15).

$$M_{CR} = \frac{w(N\mu - (m_r + m_e)g|sin\theta|)}{4}. \tag{2.16}$$

From here, we can make another substitution for F_F from Equ. (2.7) in Equ.(2.15). To get our final equation, Equ. (2.16) for the moment exerted by the force of friction which our robots steering servos will need to overpower to successfully steer the wheels. This equation allows the designer to specify a servo or motor which will output enough torque to successfully perform the desired function.

Lead Screw/Wheel Steering Analyses

Both analyses detail a process behind finding the required output of a servo or motor in order to perform a desired function in the design.

$$FOS = \frac{T_s}{M_{CR}}. \tag{2.17}$$

Equ. (2.17) is the FOS for this type of analysis where T_s is the torque output of the specified servo or motor in the design. A FOS of 1.25 to 2 should be sufficient to ensure that failure does not occur. Manufacturers often sell servos which do not output their marketed torque output so we recommended a minimum FOS of about 1.5 if the source is not very reliable.

2.1.4 Finite Element Analyses

For parts which will be under a considerable amount of stress, a detailed analysis and simulation can be done to gain a better understanding of how that part will take the forces and moments on it. All load bearing parts should be analyzed to ensure that they will not break, or deform under the expected loads they will be under. This type of analysis becomes particularly critical in instances where the designer wishes

to optimize their design to maximize load output for some function or to minimize something like mass.

These analyses are dependent on a variety of spacial, material and contact variables [49] as discussed in the introduction. A given part can be modified by changing its size (thickness, width, length), geometry, fixture conditions, temperature, phase type, material type or input loads to modify the results of this analysis. To start, the designer will need to create a 3D model of the part in a CAD software like Solidworks which also has the analysis tools that are utilized for this analysis.

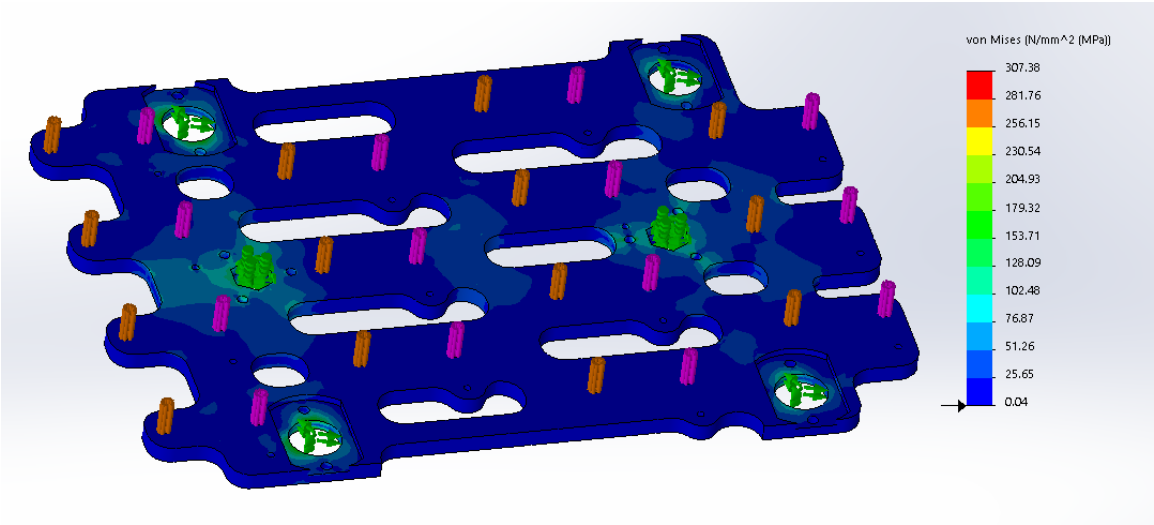

Figure 2.5: Lower plate Solidworks FEA simulation.

Fig. (2.5) shows the 3D model of the lower plate from the ARA Labs V3 robot. To perform this analysis a mesh must be created for the model which breaks up the model into a bunch of tetrahedral elements. Then, the forces and fixture conditions of the part need to be created. The green arrows represent fixture conditions in various directions depending on the arrow. The outer ones do not fix the part entirely and allow sliding up and down but not side to side. While the center two are completely fixed because that was where the plate interfaces with a set of lead screws that are used to actuate the plate up and down. The orange and pink arrows represent forces

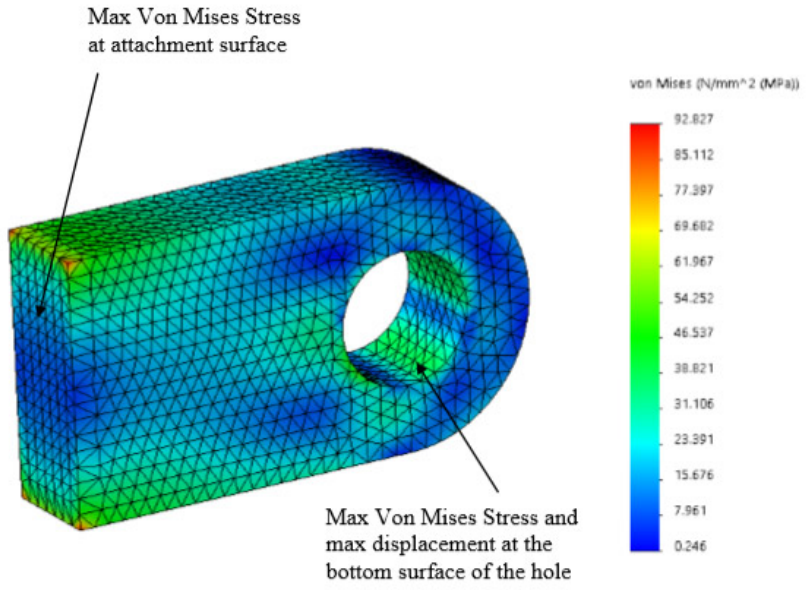

Figure 2.6: Another simulation with a visible mesh [8]

pulling on the plate from below originating from an array of permanent magnets.

$$\sigma_v = [\frac{1}{2}[(\sigma_{11} - \sigma_{22})^2 + (\sigma_{22} - \sigma_{33})^2 + (\sigma_{33} - \sigma_{11})^2 + 6(\sigma_{12}^2 + \sigma_{23}^2 + \sigma_{31}^2)]]^{\frac{1}{2}}. \tag{2.18}$$

With a model, a mesh, the correct fixture conditions, the material information and at least one external force, a simulation can be run which will result in the creation of Fig. (2.5) with the color bar on the right plotting the Von Mises stress (Equ. (2.18) experienced by the part within each tetrahedral element. Since programs are only as good as the information you put in and so many variables can significantly effect the outcome of this simulation it is recommended that the designing engineer conduct a similar analysis using a set of particular points and cross sections of interest to verify the results of the simulation with hand calculations. These verifications can be done with the mathematics discussed during the introduction of this paper and Equ. (2.18).

$$FOS = \frac{\sigma_y}{\sigma_{pmax}}. \tag{2.19}$$

The FOS for this type of analysis can be determined by finding the maximum stress experienced by the modeled part (σ_{pmax}) and dividing the yield strength (σ_y) of the material of the part by it. There is a database of material properties that already exists within Solidworks however, if the designer is using a material that is not present in the database, they can find more information (at http://www.matweb.com) and manually enter the information for a custom material. A value greater than or equal to 1.5 should be sufficient to ensure that the part does not break under expected use however, the value should be raised for particularly critical parts which may experience greater loads under special circumstances.

2.1.5 Contact Stress Analyses

A contact stress analysis is done to analyze the wheels of a robot and ensure that they will not shatter or break during typical use. This analysis builds off the the equations established from the Turn Over Analysis; to start, a summation of forces is done [50].

$$0 = 2F_{Amag} + 2F_{Bmag} - F_A - F_B. \tag{2.20}$$

Where F_A and F_B are reactionary forces acting at points A and B opposite to F_{Amag} and F_{Bmag} in Fig. (2.1). We solve for F_A to later plug into a modified version of Equ. (2.1).

$$0 = d_1(2F_{Amag}) + (d_1 + d_2)(2F_{Bmag}) - d_3 m_r g - d_1(F_A) + (d_1 + d_2)(F_B). \tag{2.21}$$

Equ. (2.21) assumes static conditions causing the M_C term to drop and be replaced by the reactionary forces acting at points A and B. From here, we can plug in Equ. (2.20) solved for F_A into Equ. (2.21).

$$F_B = \frac{2d_2F_{Bmag} - d_3m_rg}{d_2}. \tag{2.22}$$

We now solve for F_B in Equ. (2.22) to determine the reaction force acting at point B and subsequently point A with Equ. (2.20). With the reaction forces now known values, we can move on to determine the half width (b) of the contact area [51] of the wheels caused by the reaction forces acting on them in the normal direction.

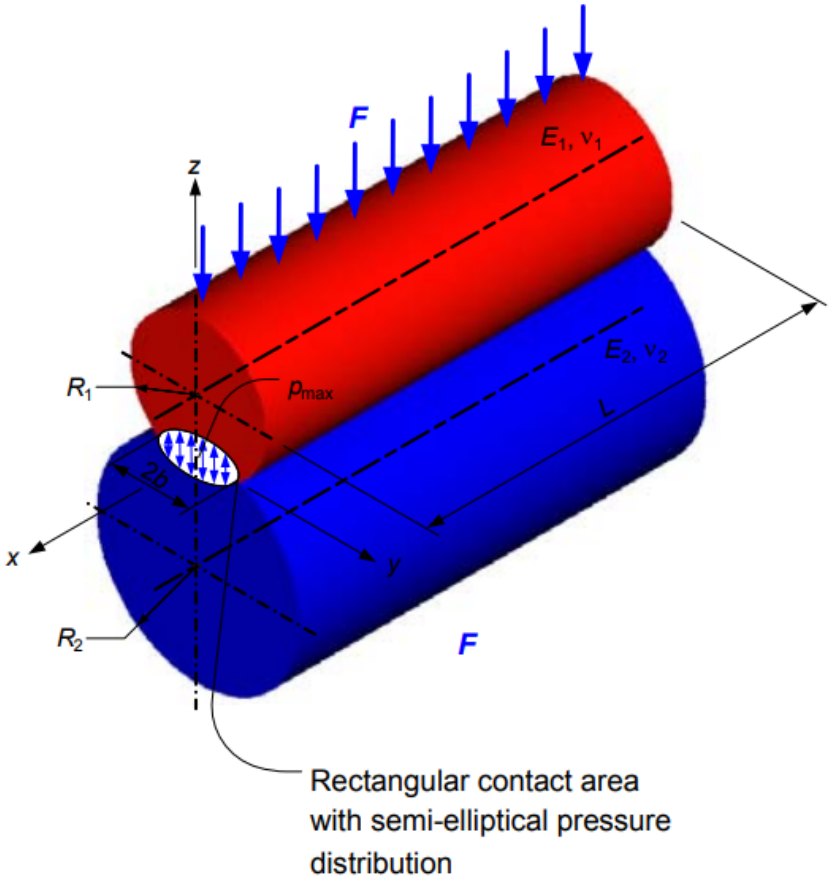

Figure 2.7: Generic contact stress diagram [9].

$$b = \sqrt{\frac{4F(\frac{1-\nu_1^2}{E_1} + \frac{1-\nu_2^2}{E_2})}{\pi L(\frac{1}{R_1} + \frac{1}{R_2})}}. \tag{2.23}$$

In Equ. (2.23), L is the width of the wheel, ν is Poisson's ratio of a material [49], E is the modulus of elasticity of the material [52,53] and F is F_A, which is the highest reactionary force acting on any of the wheels for all cases. In Fig. (2.7), to create the scenario of a plate (steel surface with subscript [$_2$]) in contact with a cylinder (rubber coated wheels with subscript [$_1$]), R_2 is set to be infinity, creating the scenario of a flat surface in contact with a cylinder (this term goes to zero and is therefore dropped).

Since neodymium magnets are quite brittle and both steel and neodymium are not very elastic, we recommend coating the wheels with a layer of rubber using an adhesive after abrading both surfaces. This allows for a much greater friction factor with the surfaces the wheels come into contact with and allows for a significantly larger contact area for the contact stress to be distributed over.

$$p_{max} = \frac{2F}{\pi L b}. \tag{2.24}$$

With the half-width Equ. (2.23), we can now calculate the contact stress on the wheels using Equ. (2.24). If p_{max} is greater than the compression strength of the structural material within the wheels, the wheels will be unable to withstand the forces exerted on them by the reaction forces. The same FOS equation as Equ. (2.19) may be used where p_{max} is substituted for σ_{pmax}. A FOS value of at least 1.75 or greater should be sufficient to ensure that the wheels do not break. When using a tougher elastic material to coat the outside of the wheels, the halfwidth will be much larger than it would be with a material such as steel. This results in the force of the wheel being distributed over a much larger effective area which then results in a

significantly lower stress since the area is larger. A large FOS of 10+ is not uncommon with an SBR rubber coating.

2.2 Expanded Analyses

2.2.1 Transformation Analyses

For the ARA Labs V3 Robot, we needed to perform an additional analysis that was an expansion of the turn over analysis. This analysis type is done to determine the amount of torque required from the output of a multi-servo and link system at each individual servo, how those servos effect each other successively and the effect this system has on the turn over analysis.

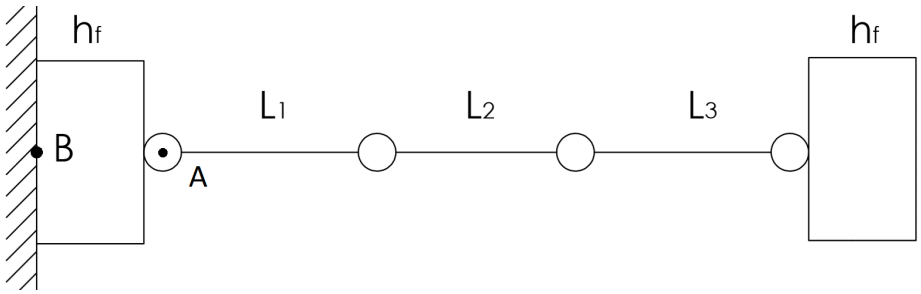

Figure 2.8: Extended statics diagram with servos at each circle and equipment mass at the midpoint of L_2.

Our V3 robot was an expansion of our V2 robot concept which essentially created a lightweight version of it and put one on each end (and called the feet) of a 6 degree of freedom arm manipulator. In Fig. (2.8), h_f represents the height of the feet, m_f is the mass of a foot and m_e is the mass of an equipment load. L_1, L_2, L_3 are the lengths of links, one through three. m_e is the mass of equipment that the robot is carrying. m_{L1}, m_{L2}, m_{L3} are the masses of their respective links. g is acceleration due to gravity.

$$\begin{aligned} M_B = (\frac{1}{2}h_f)m_f g + (h_f + \frac{1}{2}L_1)m_{L1}g \\ +(h_f + L_1 + \frac{1}{2}L_2)(m_{L2} + m_e)g \\ +(h_f + L_1 + L_2 + \frac{1}{2}L_3)m_{L3}g \\ +(\frac{3}{2}h_f + L_1 + L_2 + L_3)m_f g. \end{aligned} \tag{2.25}$$

To start, we take a moment at point B in Fig. (2.8) which creates Equ. (2.25). This equation is quite large but is simply just a summation of the various sources of moments in the system. Since each link has some mass and a certain length, each chunk of mass has its own term. The major concept to discern from this equation is the significant effect that length and mass have on a system as they get further out from the point of rotation (in this case, B). When designing our V3 robot we had to optimize the design to minimize for weight in order to create a functioning inch worm like robot.

$$\begin{aligned} M_B = (h_f + \frac{1}{2}L_1)m_{L1}g \\ +(h_f + L_1 + \frac{1}{2}L_2)(m_{L2} + m_e)g \\ +(h_f + L_1 + L_2 + \frac{1}{2}L_3)m_{L3}g \\ +(\frac{3}{2}h_f + L_1 + L_2 + L_3)m_f g. \end{aligned} \tag{2.26}$$

Since each of the elements considered in this analysis also add additional moments into the system, we should add the effect of these components to our Turn Over Analysis if the given design has a similar subset of extending components from the base (foot) of the robot. This can be done quite simply by removing the effect of the closest foots mass from Equ. (2.25) (the first term) since the mass of the foot is already taken into account in the base Turn Over Analysis; making Equ. (2.26).

$$M_C = d_1(2F_{Amag}) + (d_1 + d_2)(2F_{Bmag}) - d_3 m_r g - M_B. \tag{2.27}$$

From here, we can subtract the modified M_B from Equ. (2.26) into Equ. (2.1) to get Equ. (2.27). Please note that the terms and variables in Fig. (2.8) and Equ. (2.27) are independent from those related to Fig. (2.1) and Equ. (2.1) outside of the subtraction being done.

$$\begin{aligned} T_A = (\frac{1}{2}L_1)m_{L1}g + (L_1 + \frac{1}{2}L_2)(m_{L2} + m_e)g \\ +(L_1 + L_2 + \frac{1}{2}L_3)m_{L3}g \\ +(L_1 + L_2 + L_3 + \frac{1}{2}h_f)m_f g. \end{aligned} \tag{2.28}$$

We can also performing this analysis at point B to obtain Equ. (2.28). This allows us to calculate the required torque output of a servo positioned at the top of a foot in a given design. The same translation can be done to find the torques required at each of the successive points in Fig. (2.8) This is important to the designer because it allows them to specify a particular piece of equipment which will be able to fulfill the given designs needs.

For FOS determination, please refer to the Equ. (2.3) and Equ. (2.17) respectively. For the turn over analysis, be sure to use modified moment equation. In this modified scenario, achieving a high FOS might be cost prohibitive and too bulky for the needs of the given system. Typically, this will be the bottle-necking constraint for a design of this type so, the design should be optimized to maximize the turn over analysis FOS in applicable designs.

2.2.2 Impact Contact Stress Analyses

The purpose of this analysis is to gain a better understanding of the durability of the given robots wheels to determine if it could directly be applied to a steel surface or if it would require an additional tool like a ramp to prevent breakage from occurring. To perform this analysis, we need to calculate how quickly the robot would be moving, up until it impacts the steel using dynamics [54].

$$V_{height} = \sqrt{2gh}. \tag{2.29}$$

$$V_{mag} = \frac{1}{m_r} \int_0^t F_{mag}. \tag{2.30}$$

The two major contributing elements to the robots velocity at the time of impact are the height at which the robot is dropped from (Equ. (2.29)), and the relative pull strength of the neodymium magnet at some distance h at time t (Equ. (2.30)). Assuming that the robot starts with no initial velocity and at a distance that is further than the magnets pull range ($F_{mag} = 0$ at $t = 0$). The velocity at $h = 0$ can be calculated by summing the velocity added by the force generated from the magnetic field (V_{mag}) and the velocity added through acceleration due to gravity (V_{height}).

$$V_{mag} = \frac{3F_{mag}t}{4m_r}. \tag{2.31}$$

To simplify ($F_{mag} = f(h)$) we make two assumptions, that the force of the magnetic field is a constant equal to $\frac{3}{4}F_{mag}$ and that the duration of time F_{mag} acts to accelerate the wheel before impact is 0.1s. This allows us to simplify the V_{mag} equation and calculate the robots initial velocity (V_i) going into the impact.

$$V_i = V_{height} + V_{mag}. \tag{2.32}$$

After determining the initial velocity of the robot going into an impact with a steel plate with Equ. (2.32), we need to calculate the average force that would act on the robot over the duration of the collision. The generic equation for impulse momentum is as follows:

$$\int_0^t F dt = m_r V_f - m_r V_i. \tag{2.33}$$

$$F_{avg} \triangle t = -m_r V_i. \tag{2.34}$$

Since the magnet is strongly attracted to the steel surface and the steel plate is not going to move, the ARA team can assume that the impact occurs over a very small amount of time (approximately 0.0001s). We also know that the final velocity of the robot V_f will be 0 since both objects will not be moving at the end of the collision, allowing us to simplify Equ. (2.33) into Equ. (2.34).

With the average force, which acts on the wheels during the course of the robots impact with the steel plate, we can now substitute F with F_{avg} in Equs. (2.23) and (2.24) to calculate the stress, which acts on the wheels from height h. When solving for h_{max} the following equation is obtained by utilizing Equs. (2.23), (2.24), (2.29), (2.31) and (2.34):

$$h_{max} = \frac{(\frac{\pi \sigma_c b L \triangle t}{m_r} - V_{mag})^2}{2g}. \tag{2.35}$$

Since b is dependent on F_{avg}, which is dependent on h_{max} we cannot directly solve for h_{max} using Equ. (2.35). Instead, we iteratively solve for h_{max} by creating

a program to approximate and change h_{max} slightly to converge toward a state at which $p_{max} = \sigma_c$. Where σ_c is the compression strength of the material the wheels are made of and p_{max} is from Equ. (2.24).

When working with strong magnets with a collective pull strength of greater than $200N$, the distance at which it becomes difficult to control can reach over a few cm ($2.5cm$). Even more so with very strong magnets like those found on our V2 and V4 robots with total pull strengths around $5000N$. These robots often become difficult to control and overpower the magnetic strength by hand (h_{ctrl}) at a distance of up to $15cm$. When considering the FOS for this analysis, h_{max} should be a greater than h_{ctrl} for a much sturdier robot that can more easily be placed on surfaces to begin inspection. If h_{max} is less than h_{ctrl} than a ramp would be required to safely adhere the robot to a surface to begin inspection which has the added consequence of making it significantly more difficult to place the robot on a surface which it would be operating upside-down.

$$FOS = \frac{h_{max}}{h_{ctrl}}. \tag{2.36}$$

A FOS of 1.5 to 2.5 should be sufficient to ensure the structural integrity of the wheels design. The same equation may be used from Equ. (2.36).

2.2.3 Robotic Maneuverability

When designing a robot, it is important to consider how the designer wishes for their robot to maneuver around its intended environment. For this, we recommend a conventional approach with robotic kinematics [55]. For instance, our V4 robot has been designed to have four independently steerable magnetic wheels. This configuration of wheels allows our robot to take advantage of a variety of advantageous steering

configurations such as Ackermann, Synchronous, and Static-Point Steering.

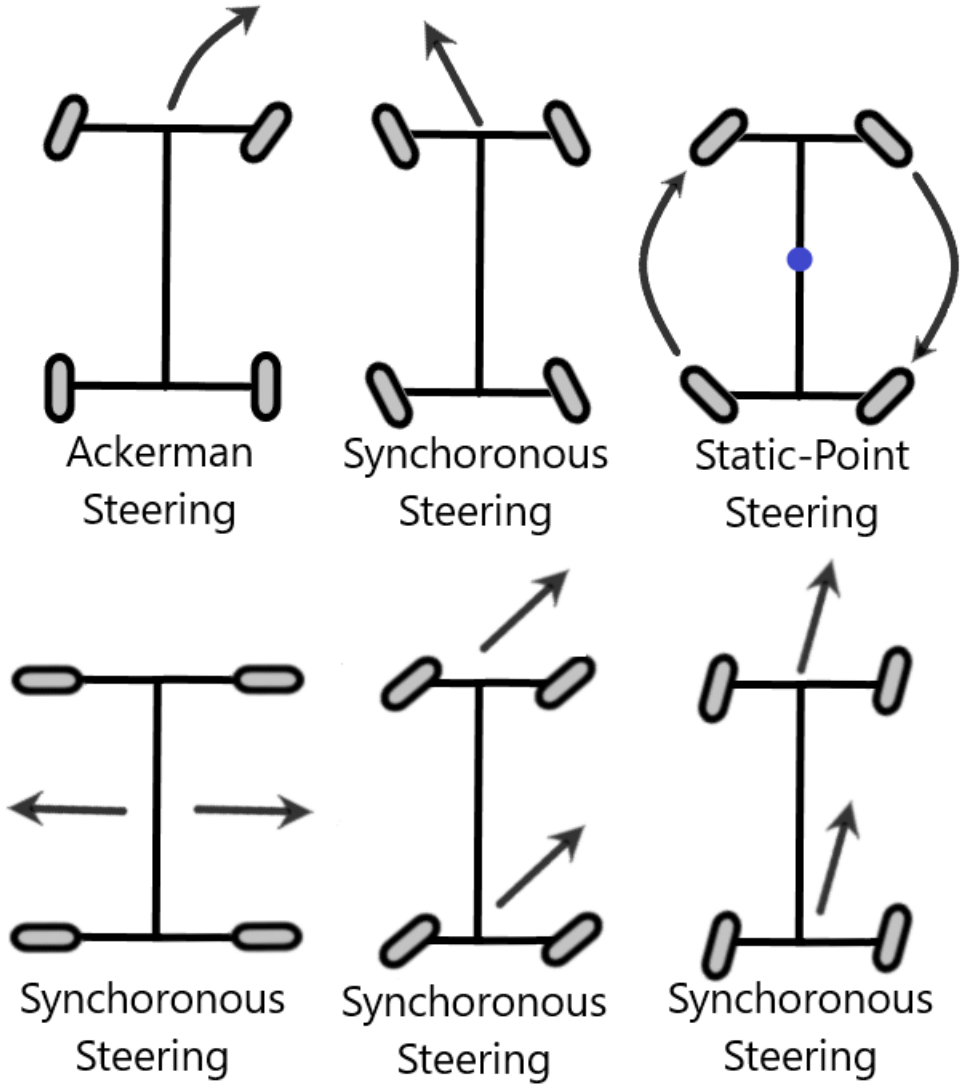

Figure 2.9: V4 robots steering configurations.

These allow our V4 robot to be particularly adept at navigating awkward and uneven terrains found on steel structures through its ability to utilize each of the steering types shown in Fig. (2.9).

Per Muir's approach in their paper with eqs. 3.40, 3.41 and 3.42 [55]. Our robots degree of mobility (δ_m), steerablity (δ_s) and maneuverability (δ_M) can be determined.

$$\delta_m = 3 - rank[C_1(\beta_s)]. \tag{2.37}$$

$$\delta_s = rank[C_{1s}(\beta_s)]. \tag{2.38}$$

$$\delta_M = \delta_m + \delta_s. \tag{2.39}$$

The C matrix is a representation of the robots constraints and β_s is a vector that describes the steering angles of each of the robots wheels.

With proper control mechanisms, it can be ensured that each of the wheels axes intersect at one point; creating an instantaneous center of rotation (ICR). This is the point which the robot will pivot around while moving. When this condition is met, our V4 robot has a degree of mobility of one, a degree of steerablity of two. Which results in our robot scoring a three in its degree of maneuverability. This means the ICR of our robot is not constrained at all on the surfaces it navigates upon.

It is important to note that robots with the same degree of maneuverability are not necessarily maneuverable in the same manner since the degree of maneuverability of a robot is made up of both its degree of steerability and degree of mobility. What this means is that each wheel set in a design poses its own set of advantages and constraints. The designer should consider at length about the different possible configurations and choose the one which will enable the robot to navigate with the best capabilities for its intended purpose.

2.2.4 Wheel Obstruction Analyses

A Wheel Obstruction Analysis is done to mathematically determine the amount of torque required in a wheel for it to scale up a ledge of height h. Since this analysis is dynamic [56], the sum of all forces and moments do not equal zero like in the static cases. To start, we need to analyze the relationship that the diameter of the wheel and the height of the ledge have on the torques generated.

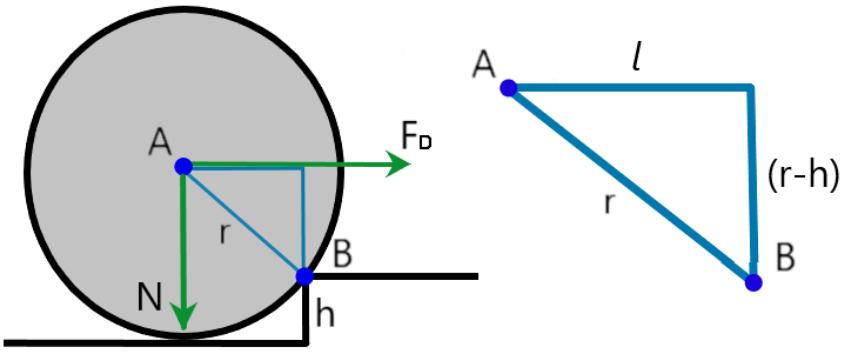

Figure 2.10: Edge obstruction diagram, [left] zoomed in portion [right].

At the instance the wheel comes into contact with a ledge, it has a contact point B at height h in Fig. (2.10). This point is the point which the wheel will need to pivot around for the wheel to scale a hypothetical ledge.

$$\tau_F = F_D(r-h), (CW). \tag{2.40}$$

$$\tau_B = \frac{Nl}{4}, (CCW). \tag{2.41}$$

We draw a triangle between the center of rotation of our wheel and contact point B. From here, the forward (τ_F) and backward (τ_B) torque equations about B can be written as Equs (2.40) and (2.41).

$$l = \sqrt{2rh - h^2}. \tag{2.42}$$

We use the Pythagorean theorem to solve for the distance l in Equ. (2.42) using the right side of Fig. (2.10) CW means the clockwise direction and CCW means the torque is in the counter clockwise direction. Since this is an analysis of one wheel, N is divided by the number of wheels.

$$F_D = \frac{N\sqrt{2rh - h^2}}{4(r - h)}. \tag{2.43}$$

When the torque in the forward direction (τ_F) is greater than the torque in the backward direction (τ_B) the wheel will be able to scale the ledge. By setting these two equations equal to each other and solving it for the required force to drive the robot forward (F_D) and up the ledge, Equ. (2.43) can be written.

$$F_D < \frac{F_F}{4}. \tag{2.44}$$

The designer should take a moment to ensure that Equ. (2.44) is true. If this statement is not true, slipping will occur in the wheels and the robot will cease to drive itself forward at this threshold; instead the wheels will rotate in place.

The major insight to be gained from Equ. (2.43) is that the friction force required to scale the ledge increases toward infinity as h approaches r. However, in our case since our wheels are magnetic, and we are assuming that the surface material is steel, at $h = r$ the problem simplifies since the magnet attracts into both steel surfaces, a new point of rotation occurs at point B. From here, rolling will take place as it normally would along a steel surface were the turning pushes the wheel into the new surface and generates a large increase of the normal force acting at point B when $h = r$. This causes the wheel to beginning rolling up the surface h creates and is how

our robots are able to travel over internal edges in steel. In the case that the ledge is not a magnetic material, we can now determine mathematically if our robot will be able to generate enough torque in its the wheels to scale a given ledge which does not interact with the ring magnets.

$$FOS = \frac{\tau_m}{rF_D}. \tag{2.45}$$

A FOS for this analysis in Equ. (2.45) is written as a relationship between the required F_F or F_D (whichever is the limiting value) and the maximum torque output of the driving motor. Where τ_m is the torque output of the motor. So long as the FOS value is greater than about 1.1, the designer can be confident that their design will be able to perform the desired function. It should be noted that the same note made at the end of the Lead Screw/Wheel Steering analyses about motor/servo output should still be taken into account. Therefore, if purchasing from an more unreliable source, a FOS of 1.5 might be more appropriate.

2.3 Summary

The detailed analyses discussed in this chapter provides a framework for analysis of climbing mobile robots that will assist a designing engineer in ensuring their design will function as intended and allow them to quantify the factors of safety of their design. A designer can use the discussions within this framework to analyze and inform their own design decisions. The application of this framework during design can help the design go through less iteration, failures and reduce total cost by ensuring that parts will perform their functions successfully but are not over specified for their intended purpose. A designer equipped with this knowledge may also utilize it to optimize their own designs in instances of particularly demanding design

requirements.

Chapter 3

Application of Framework

3.1 Robot Design and Application of Framework

3.1.1 V2

The ARA Labs V2 Robot concept and design was made by the ARA Lab's members [36,57–59]. The V2 robot was created to be sturdy, simple to use, and to be outfitted with additional equipment.

Overall, the V2 robot in Fig. 3.1 consists of an aluminum frame and a scanning frame made of hardened steel rods. The frame has a belt system on it used to maneuver an eddy current probe around a scanning area. There are four large ring magnets, which makeup the inside of the robots wheels. Each magnet generates an attractive force of 1126.7 N. On top of the frame above the wheels lies the computer, which controls the systems motors, camera and stepper motors. On the very top is where the NORTEC 600 rests securely, it is a device for eddy current flaw detection. When scanning, the eddy current probe is moved in a line-by-line pattern throughout the scanning area. The robot is powered with LiPo batteries and has a run time of

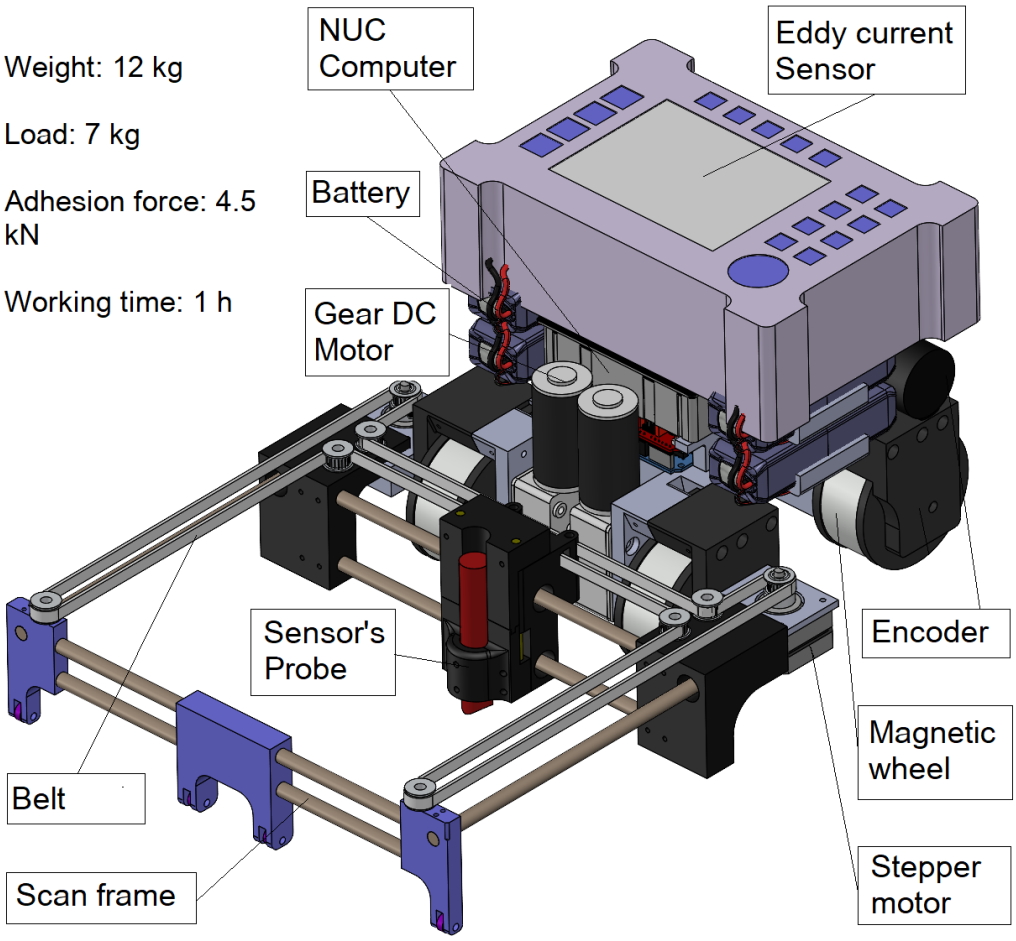

Figure 3.1: CAD model and specifications of the proposed ARA robot.

60 minutes before needing to recharge.

The V2 robot has an aluminum frame that spreads over of an area of $20.5cm \times 18.7cm$ with a thickness of $1.2cm$ or greater. The scanning area is $17.6cm \times 16.76cm$ and the whole robot has a footprint of $45.65cm \times 31.2cm \times 21.73cm$.

Figure 3.2 shows the electrical structure and connectivity of the proposed robot, which is equipped with four servos, two encoders, an IMU, a camera, a NUC computer running ROS, and a NORTEC 600. There are two boards, the main which controls the wheels of the robot and receives the encoder and IMU data, and the sensor board which controls the motors which allow the robot to scan with the eddy current sensor from the NORTEC 600. The electrical components are powered by 11.1 V lithium

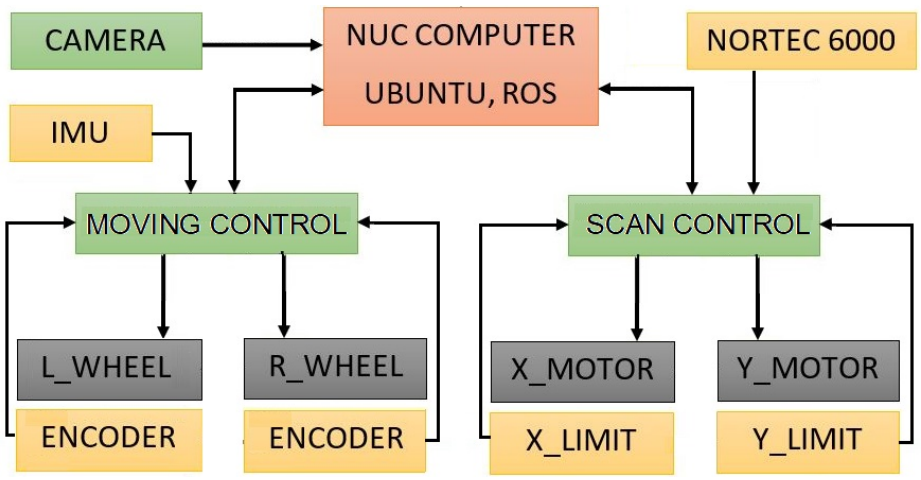

Figure 3.2: Electrical hierarchy of the V2 robot

polymer batteries.

This robot was designed and fabricated just before 2019, as a result the framework was used to analyze the created design. The analyses of the design thresholds of our V2 robot begin with a turn over analysis. Once the maximum theoretical equipment load is determined, a contact stress analysis is performed to determine the failure mechanics of the designed robots wheels. Finally, a sliding fiction analysis is performed with the turn over analysis results. Our V2 Robot has a FOS against turning over of 7.82, a contact stress analysis FOS of 2.54, and a static friction FOS of 15.87.

3.1.2 V3

The design of the hybrid climbing robot by the ARA Lab's members [43] is illustrated in Fig. (3.3) and it's function is described in Fig. (3.4). The robot is divided into two main parts: the feet and the body. In mobile mode the magnets hover in an untouched position with a 1mm distance from the steel surface. The magnets are ring shaped and arranged in an array, which allows the robot to pass nuts and bolts smoothly while still maintaining a full adhesion force. The torsion spring is instrumental in the design of the feet, they allow a given magnet cell to individually adapt to varying

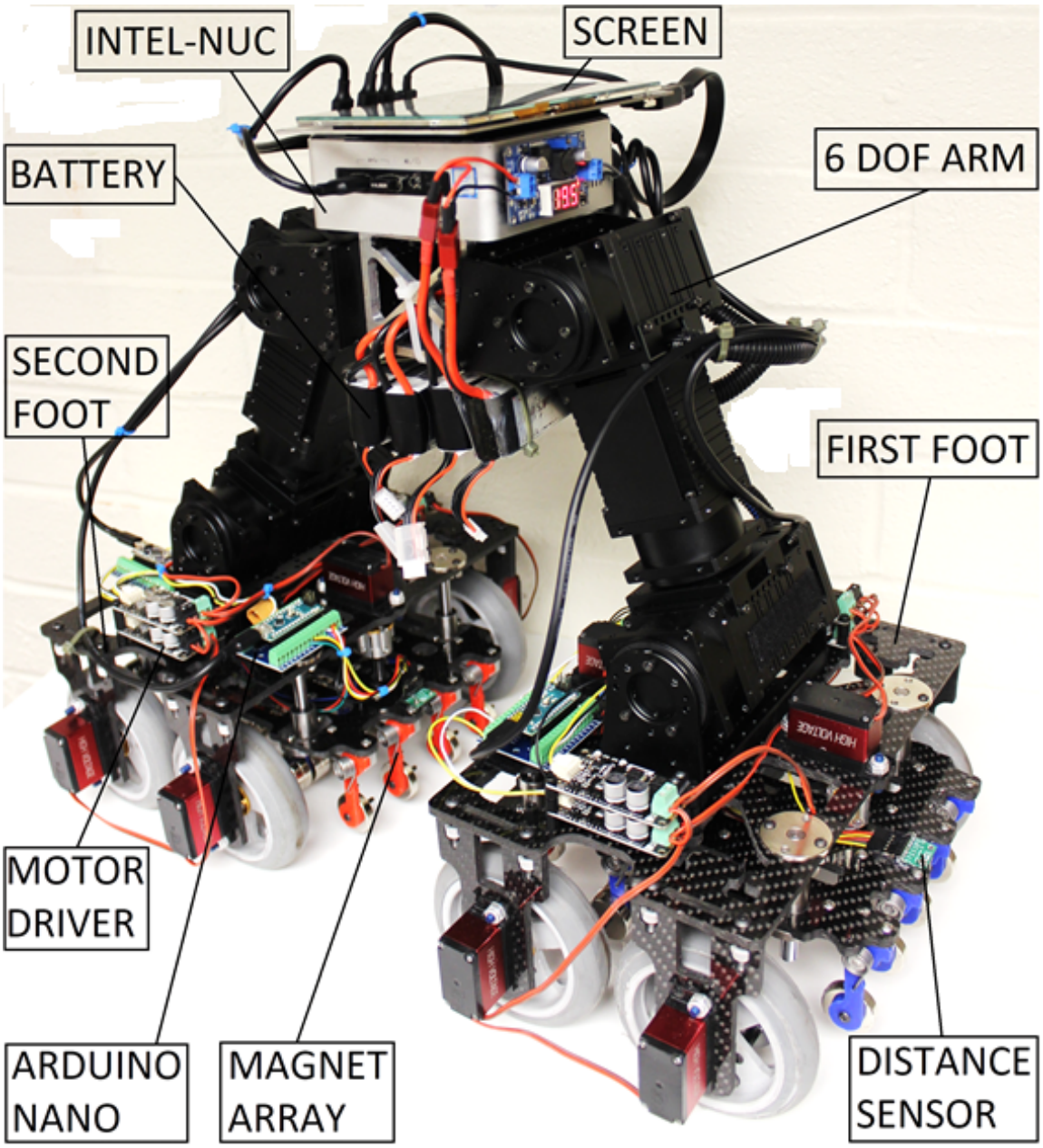

Figure 3.3: Picture of the V3 robot.

external stimuli and then return to its initial structure within the array.

The distance between the magnet arrays and surface is controllable and each foot is able to work in touched or untouched orientations. Two parallel feed screws are utilized with an actuator to enable the control system to modify the distance each foot is kept at. Feedback from a distance sensor helps to ensure that the magnet arrays

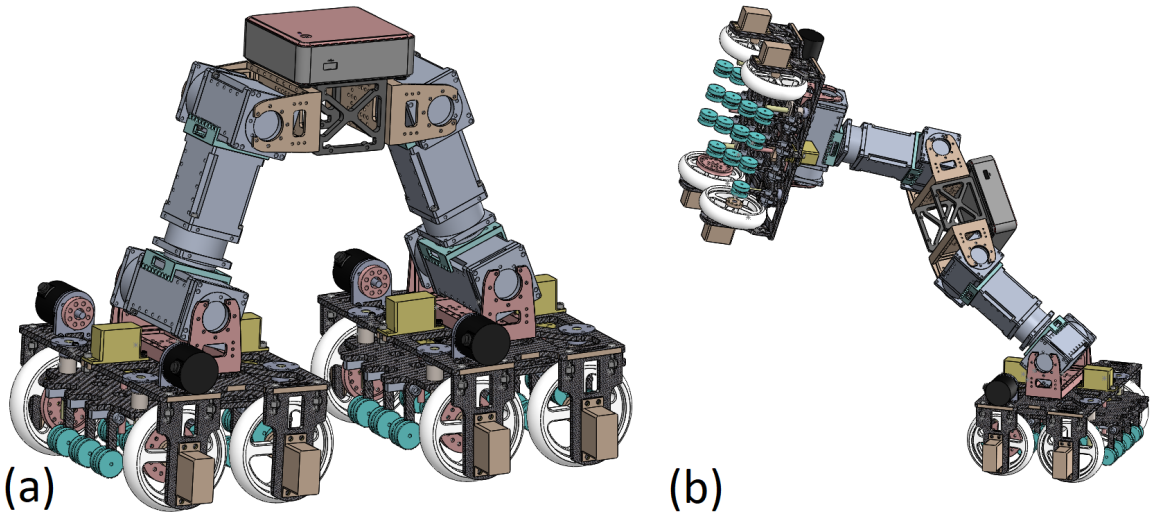

Figure 3.4: Robot function (a) mobile mode; (b) transforming/worm mode

are kept at an optimal distance. Four wheels on each foot keep the robot stable when standing on one foot and support large moments while being light weight. The rubber wheels maximize the friction factor between the robot and the surfaces each foot is adhered to. The foot design allows the ARA to robot function on different surface conditions. The body has 6 degrees of freedom (DOF) and functions like a robot arm as shown in Fig. (3.4).

When the robot encounters an area it is having difficulties traversing while in mobile mode, the robot will shift into transforming mode to find a new surface in order to continue along it's task. In transforming mode one foots magnet array will touch fully to the surface to maximize its adhesion force. Then the magnets on the second foot will move up to release the adhesion force. Now, robot works as a 6 DOF robot arm. When touching a new surface, the process happens again to the opposite feet. This enables the robot to move the whole robot to new place. The whole process is shown in Fig.3.7.

The framework proposed this thesis was started on with the design of the V3 robot with Son Nguyen. We faced major challenges in creating our V3 robot due to

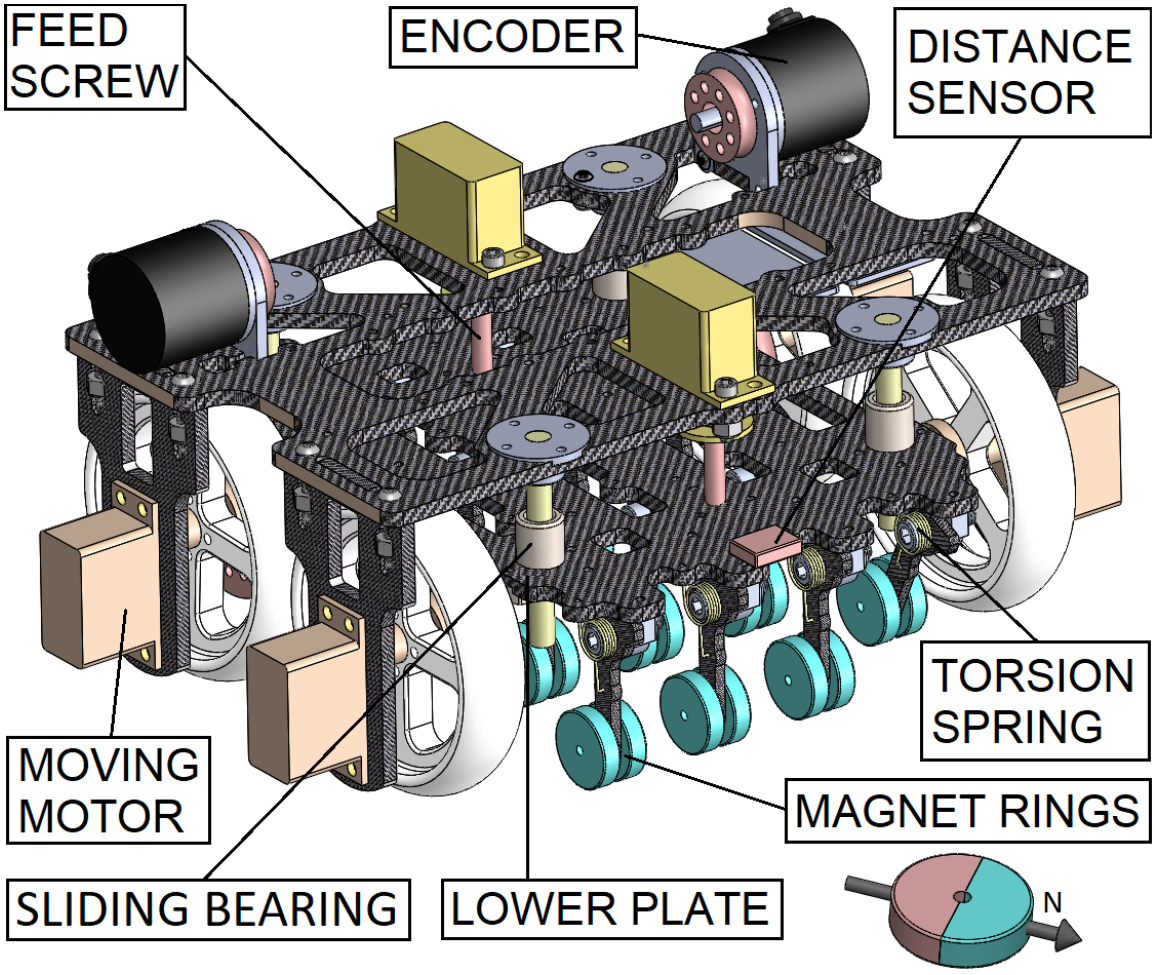

Figure 3.5: Robot foot with flexible magnet array.

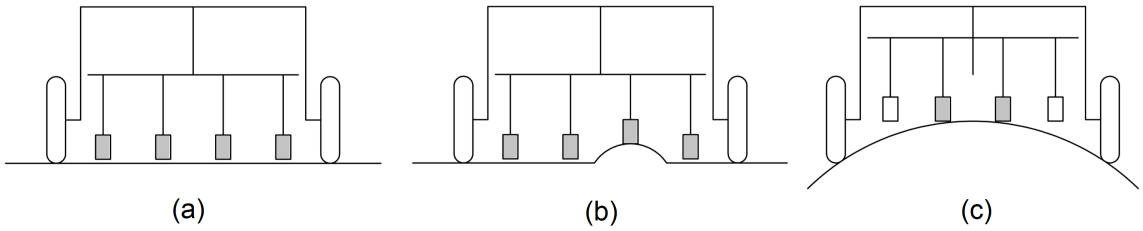

Figure 3.6: (a) Robot on flat surface; (b) Robot passing an obstruction; (c) Robot on curving surface.

the particularly demanding design concept of having a 6 DOF arm manipulator as the body of the robot. Creating a robot capable of performing this type of moment posed quite a few challenges to creating a functional design. Namely, it became abundantly clear that mass in the feet of the robot would be a critical factor that we

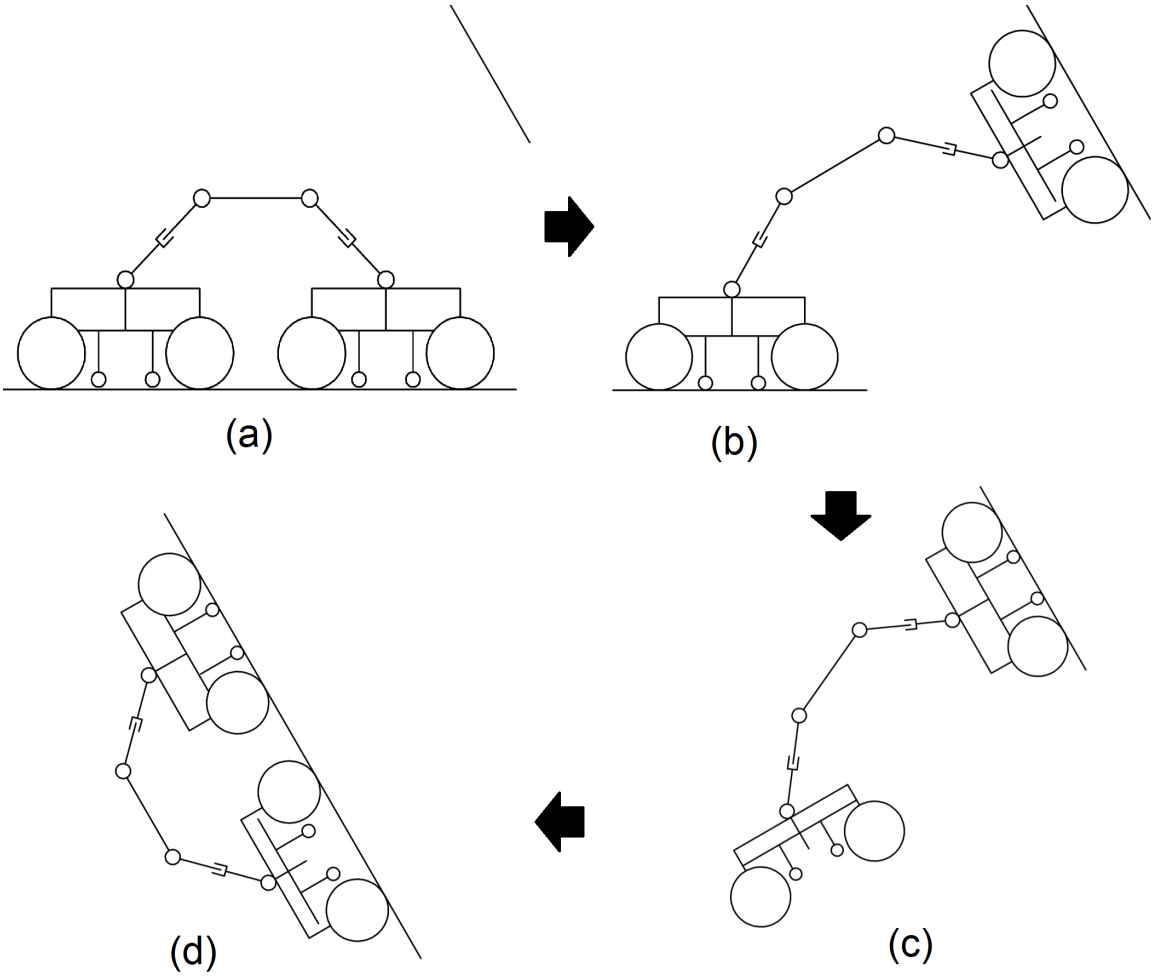

Figure 3.7: Transformation process: (a) robot in mobile mode; (b) robot touches 1st foot to old surface and looks for new one; (c) the 2nd foot touches to a new surface and moves the other side; (d) robot returns to mobile mode on the new surface.

had to minimize in order to allow our V3 Robot to function as intended. We started by performing a transformation analysis which mathematically put the effect of mass and distance into terms for our robot. Based on the results from our initial transformation analysis we determined that our robots motors would not have enough torque output to function because the feet of the robot weighed too much. Our detailed analysis was capable of allowing us to determine that the robot would fail before we made it.

To reduce the mass of the feet, we changed the major structural material of the feet from solid aluminium to carbon fiber and performed an FEA analysis on the parts to

determine what thickness we needed to ensure that the structural components would not break under the loads they would experience during use. Once done, we moved on to perform turn over and sliding friction analyses which allowed us to verify that the robot would not fail in these manners either. Finally, we did an analysis of the torque output required from our servos turning the lead screws of the feet of our V4 robot. This analysis allowed us to purchase servos that we knew would be strong enough to raise the lower assembly by turning of the lead screws. For additional design details, please refer to our paper: A Practical Climbing Robot for Steel Bridge Inspection [43].

3.1.3 V4

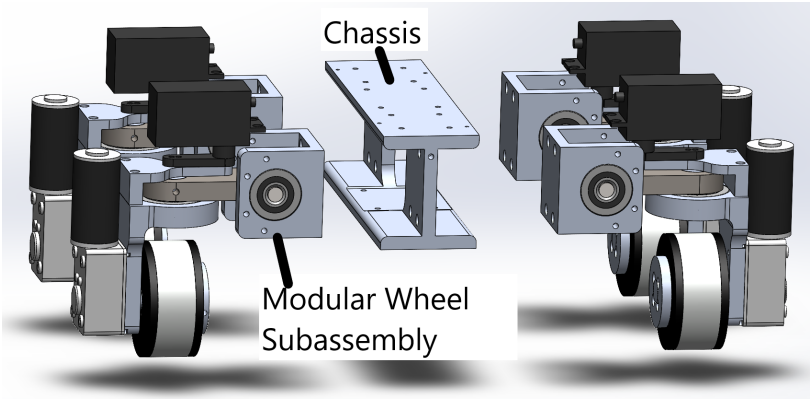

Figure 3.8: Exploded CAD model showing distinction between modular Wheel subassemblies and the chassis.

The design of our V4 robot [60] has a chassis made of an aluminium I-beam and four modular wheel subassemblies attached to it as shown in Fig. (3.8). Each of these wheel subassemblies are completely independent from one another and allow the robot to utilize different steering methods to travel along a surface.

Since the objectives for this design were to maintain the strength and reliability of one of our previous robots [61] while increasing maneuverability to do what other

Figure 3.9: Examples of Steel Substructures found on Steel Bridges.

robots couldn't. We decided that the approach to make each wheel independently steerable was the best way to develop a robot which could accurately travel along and between steel surfaces for inspection such as those shown in Fig. (3.9)

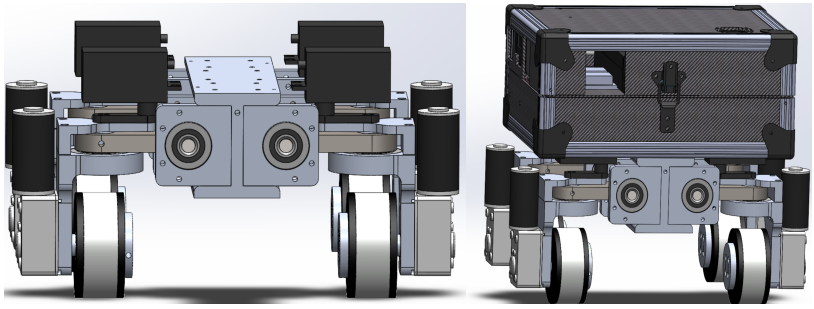

Figure 3.10: CAD model of the V4 robot.

The V4 robot is be able to traverse long continuous steel surfaces commonly found on steel bridges such as those shown in Fig (3.9). With the robots ability to take advantage of different types of steering configurations, our robot is significantly more capable of reaching more precise locations with particular orientations. This

allows the robot to be more capable of utilizing on-board inspection equipment more effectively. The steering modes also give the controller of the robot additional methods to interact and move our robot in a manner which is most intuitive to them.

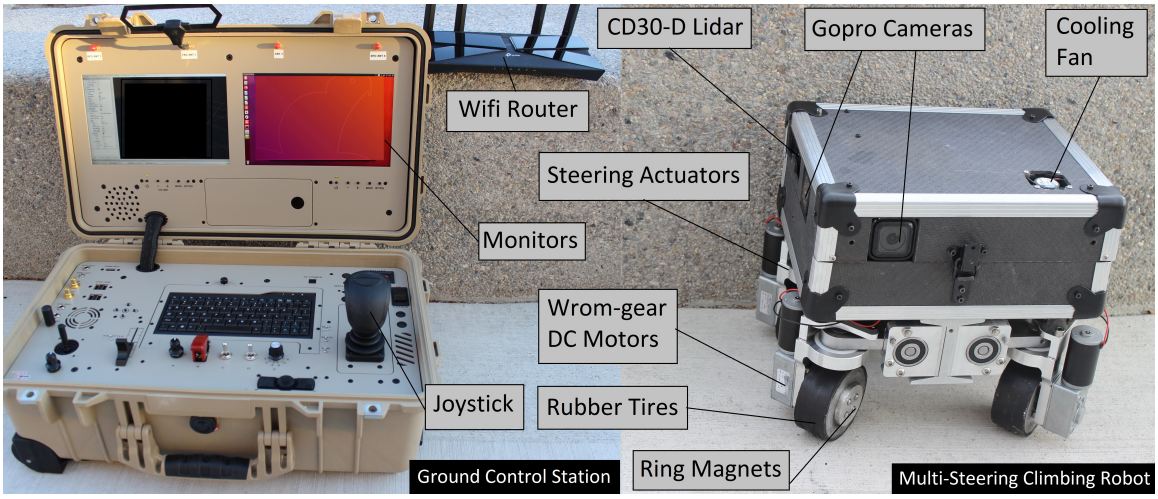

Figure 3.11: Picture of the GCS (left) and the robot (right) side by side with parts labeled.

The V4 robot has two independent channels of for teleoperation and monitoring. The data from Lidar and cameras is processed by a Dell Optiplex computer then transferred to Ground Control Station (GCS) for live monitoring. For remote control, Rx receives commands from operator via GCS's joystick. An Arduino Mega processes this signal and exports outputs to move the motors and steering servos via power amplifiers. The GCS performs localization, object detection, and visualizes the received data online on its two screens. We use an Intel NUC i7 as the computer for the GCS.

The ARA Lab robot is capable of traveling through internal and external edges on steel structures and has a spacial footprint of $33cm$ by $22.65cm$ by $30.38cm$ (width, depth, height) as shown in Fig. (3.11). The wheels have a diameter of $7.62cm$ and a width of $3.55cm$. It weights $18.14kg$.

This robot was designed through the application of the framework, before being

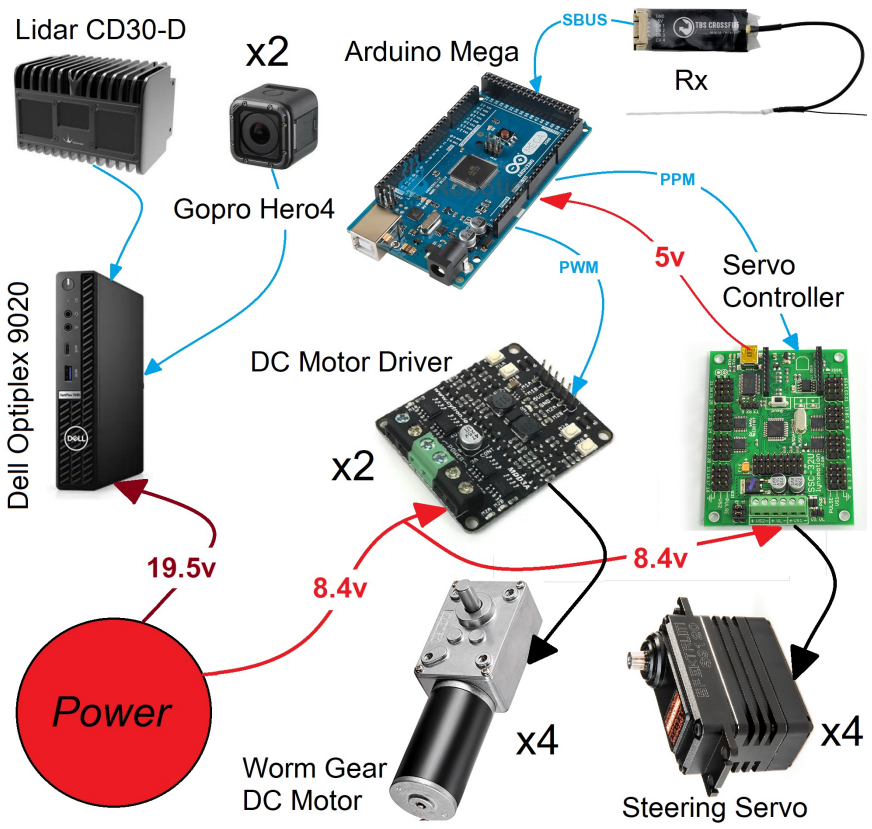

Figure 3.12: A representation of the electric system on the V4 robot.

built, we were able to use this framework to ensure that the design would not fail in any of the scenarios discussed in the framework. Through these analyses we determined that our base V4 robot has a the following FOS values: A 6.13 against turning over, a static contact stress FOS of 17.5, a sliding friction FOS of 5.29, a wheel steering FOS of 2.85, and a FOS of 1.45 for wheel obstruction ($h = .5cm$). After testing, we found that our V4 robot functioned as intended. Further results and details can be seen in the IROS 2021 Paper: Design of A High Strength Multi-Steering Climbing Robot for Steel Bridge Inspection [60].

3.2 Summary

The framework proposed in thesis equips members from the computer science community with improved ability to engineer and design climbing mobile robots. It discusses the details behind the analysis of climbing mobile robots and will assist future engineers in their efforts to design robotic platforms. As shown, this framework can serve as an effective set of analyses to design and fabricate climbing robotic platforms which allows a designer to quantify the level of tolerance that exists within their design through factors of safety.

Chapter 4

Conclusion and Future Work

4.1 Conclusion

This thesis has created a framework for analysis and design of magnetic climbing robotic systems that mathematically solves a variety of design problems and can be used to standardize the approaches future members of the computer science and industry field should take when designing their own robotic solutions for magnetic climbing mobile robots.

The framework derives 10 interconnected analyses which together, create a framework of analysis for magnetic climbing mobile robots. These analyses are as follows:

- Turn Over Analysis
- Sliding Friction Analysis
- Lead Screw Analysis
- Wheel Steering Analysis
- Transformation Analysis

- Finite Element Analysis
- Contact Stress Analysis
- Impact Contact Stress Analysis
- Robotic Maneuverability Analysis
- Wheel Obstruction Analysis

Through the application of this framework, future designers of these type of robots can approach their research project with the basis that this thesis develops. This framework can reduce the time needed to draft and finalize a design concept and consequently will help to reduce the typical costs incurred by the educated trial and error based methods used in the past. Engineers designing a robotic platform of this type can build off of the base framework created by this thesis and mathematically quantify their confidence in their design work through the use of the factors of safety.

This framework has been created and applied through the creation of the ARA Lab's V3 and V4 Robots. The success of these two robots is evidence of the frameworks ability to shape and inform design decisions during the creation of new robotic platforms.

4.2 Future Work

This framework defines a baseline standard of design for magnetic climbing mobile robots however, it is not all encompassing. There is room for future work in expanding the breadth of this framework to include analyses which would allow a designer to accommodate other external load cases such as the effect a robotic arm would have on the system. Work should also be done to expand this framework to include other methods of adhesion such as suction based solutions.

Bibliography

[1] K. Y. Ma, P. Chirarattananon, and R. J. Wood, "Design and fabrication of an insect-scale flying robot for control autonomy," in *2015 IEEE/RSJ International Conference on Intelligent Robots and Systems (IROS)*, 2015, pp. 1558–1564.

[2] T. Murray, "The economic cost of the [i35w] bridge collapse," 2007. [Online]. Available: https://commons.wikimedia.org/w/index.php?curid=774418

[3] US-Navy, "I35 bridge collapsed divers," 2007. [Online]. Available: https://www.dvidshub.net/image/54829

[4] P. Ward, P. Manamperi, P. R. Brooks, P. Mann, W. Kaluarachchi, L. Matkovic, G. Paul, C. H. Yang, P. Quin, D. Pagano, D. Liu, K. Waldron, and G. Dissanayake, "Climbing robot for steel bridge inspection: Design challenges," in *Austroads Publications Online, ARRB Group*, 2015.

[5] Y. Takada, S. Ito, and N. Imajo, "Development of a bridge inspection robot capable of traveling on splicing parts," *Inventions*, vol. 2, no. 3, 2017. [Online]. Available: https://www.mdpi.com/2411-5134/2/3/22

[6] Inhabitat-Author, "Helical robotics introduces climbing robots for wind turbine inspection," 2013. [Online]. Available: https://inhabitat.com/helical-robotics-introduces-climbing-robots-for-wind-turbine-inspection/

[7] T. J. Teo, G. Yang, and I.-M. Chen, *Compliant Manipulators*. Springer, 03 2014, pp. 1–64.

[8] M. K. H, "Mesh convergence in solidworks simulation," 2020. [Online]. Available: https://ckonnect.in/solidworks/mesh-convergence-solidworks-simulation/

[9] Zhu, "Tutorial on hertz contact stress," https://wp.optics.arizona.edu/optomech/wp-content/uploads/sites/53/2016/10/OPTI-521-Tutorial-on-Hertz-contact-stress-Xiaoyin-Zhu.pdf, December 2012.

[10] H. Sayyaadi, H. Kouhi, and H. Salarieh, "Control of car-like (wheeled) multi robots for following and hunting a moving target," *Scientia Iranica*, vol. 18, no. 4, pp. 950–965, 2011. [Online]. Available: https://www.sciencedirect.com/science/article/pii/S1026309811001209

[11] K. Rebai, O. Azouaoui, M. Benmami, and A. Larabi, "Car-like robot navigation at high speed," in *2007 IEEE International Conference on Robotics and Biomimetics (ROBIO)*, 2007, pp. 2053–2057.

[12] S. T. Nguyen, H. Nguyen, S. T. Bui, V. A. Ho, and H. M. La, "Multi-directional bicycle robot for steel structure inspection," in *arXiv, cs.RO, 2103.1152*, 2021.

[13] W. Budiharto, V. Andreas, J. S. Suroso, A. A. S. Gunawan, and E. Irwansyah, "Development of tank-based military robot and object tracker," in *2019 4th Asia-Pacific Conference on Intelligent Robot Systems (ACIRS)*, 2019, pp. 221–224.

[14] S. T. Nguyen and H. M. La, "A climbing robot for steel bridge inspection," *Journal of Intelligent and Robotic Systems (In Press)*, 2021.

[15] W. Myeong, K. Jung, S. Jung, Y. Jung, and H. Myung, "Development of a drone-type wall-sticking and climbing robot," in *2015 12th International Conference on Ubiquitous Robots and Ambient Intelligence (URAI)*, 2015, pp. 386–389.

[16] T. Li, Z. Zou, G. Mao, X. Yang, Y. Liang, C. Li, S. Qu, Z. Suo, and W. Yang, "Agile and resilient insect-scale robot," *Mary Ann Leibert Inc.*, vol. 6, no. 1, pp. 133–141, 2019, soft Robotics. [Online]. Available: https://www.liebertpub.com/doi/10.1089/soro.2018.0053

[17] J. Bay, "Design of the "army-ant" cooperative lifting robot," *IEEE Robotics Automation Magazine*, vol. 2, no. 1, pp. 36–43, 1995.

[18] D. Stilwell and J. Bay, "Toward the development of a material transport system using swarms of ant-like robots," in *[1993] Proceedings IEEE International Conference on Robotics and Automation*, 1993, pp. 766–771 vol.1.

[19] L. Tudose and C. Budaciu, "Design and implementation of a butterfly robot system," in *2019 24th IEEE International Conference on Emerging Technologies and Factory Automation (ETFA)*, 2019, pp. 1665–1668.

[20] P. Phamduy, R. LeGrand, and M. Porfiri, "Robotic fish: Design and characterization of an interactive idevice-controlled robotic fish for informal science education," *IEEE Robotics Automation Magazine*, vol. 22, no. 1, pp. 86–96, 2015.

[21] T. Seo and M. Sitti, "Tank-like module-based climbing robot using passive compliant joints," *IEEE/ASME Transactions on Mechatronics*, vol. 18, no. 1, pp. 397–408, 2013.

[22] S. TaeWon and M. Sitti, "Under-actuated tank-like climbing robot with various transitioning capabilities," in *2011 IEEE International Conference on Robotics and Automation*, 2011, pp. 777–782.

[23] D. Xu, X. Gao, X. Wu, N. Fan, K. Li, and K. Kikuchi, "Suction ability analyses of a novel wall climbing robot," in *2006 IEEE International Conference on Robotics and Biomimetics*, 2006, pp. 1506–1511.

[24] H. M. La, N. Gucunski, K. Dana, and S.-H. Kee, "Development of an autonomous bridge deck inspection robotic system," *Journal of Field Robotics*, vol. 34, no. 8, pp. 1489–1504, 2017. [Online]. Available: https://onlinelibrary.wiley.com/doi/abs/10.1002/rob.21725

[25] L. Nguyen, S. Gibb, H. X. Pham, and H. M. La, "A mobile robot for automated civil infrastructure inspection and evaluation," *International Symposium on Safety, Security, and Rescue Robotics (SSRR)*, 2018. [Online]. Available: https://ara.cse.unr.edu/wp-content/uploads/2014/12/Nguyen_La_SSRR2018.pdf

[26] S. Gibb, T. Le, H. M. La, R. Schmid, and T. Berendsen, "A multi-functional inspection robot for civil infrastructure evaluation and maintenance," in *2017 IEEE/RSJ International Conference on Intelligent Robots and Systems (IROS)*, 2017, pp. 2672–2677.

[27] N. Gucunski, S.-H. Kee, H. La, B. Basily, A. Maher, and H. Ghasemi, *Implementation of a Fully Autonomous Platform for Assessment of Concrete Bridge Decks RABIT*. Structures Congress 2015, 2015, pp. 367–378. [Online]. Available: https://ascelibrary.org/doi/abs/10.1061/9780784479117.032

[28] H. M. La, N. Gucunski, S.-H. Kee, J. Yi, T. Senlet, and L. Nguyen, "Autonomous robotic system for bridge deck data collection and analysis," in *2014 IEEE/RSJ International Conference on Intelligent Robots and Systems*, 2014, pp. 1950–1955.

[29] N. Gucunski, B. Basily, S. H. Kee, H. M. La, H. Pavardeh, A. Maher, and H. Gashemi, "Multi nde technology condition assessment of concrete bridge decks by rabittm platform," in *NDE/NDT for Structural Materials Technology for Highway and Bridges*, 2014.

[30] H. M. La, R. S. Lim, B. B. Basily, N. Gucunski, J. Yi, A. Maher, F. A. Romero, and H. Parvardeh, "Mechatronic systems design for an autonomous robotic system for high-efficiency bridge deck inspection and evaluation," *IEEE/ASME Transactions on Mechatronics*, vol. 18, no. 6, pp. 1655–1664, 2013.

[31] R. S. Lim, H. M. La, Z. Shan, and W. Sheng, "Developing a crack inspection robot for bridge maintenance," in *2011 IEEE International Conference on Robotics and Automation*, 2011, pp. 6288–6293.

[32] H. M. La, R. S. Lim, J. Du, W. Sheng, G. Li, S. Zhang, and H. Chen, "A small-scale research platform for intelligent transportation systems," in *2011 IEEE International Conference on Robotics and Biomimetics*, 2011, pp. 1373–1378.

[33] H. M. La, T. H. Dinh, N. H. Pham, Q. P. Ha, and A. Q. Pham, "Automated robotic monitoring and inspection of steel structures and bridges," *Robotica*, vol. 37, no. 5, p. 947–967, 2019.

[34] L. Van Nguyen, S. Gibb, H. X. Pham, and H. M. La, "A mobile robot for automated civil infrastructure inspection and evaluation," in *2018 IEEE International Symposium on Safety, Security, and Rescue Robotics (SSRR)*, 2018, pp. 1–6.

[35] N. H. Pham, H. M. La, Q. P. Ha, S. N. Dang, A. H. Vo, and Q. H. Dinh, "Visual and 3d mapping for steel bridge inspection using a climbing robot," in *The 33rd Intern. Symposium on Automation and Robotics in Construction and Mining (ISARC)*, July 2016, pp. 1–8.

[36] N. H. Pham and H. M. La, "Design and implementation of an autonomous robot for steel bridge inspection," in *The 54th Annual Allerton Conference on Communication, Control, and Computing,*, no. 54, 2016, pp. 556–562.

[37] S. T. Nguyen and H. M. La, "Roller chain-like robot for steel bridge inspection," *International Conference on Structural Health Monitoring of Intelligent Infrastructure*, 2019. [Online]. Available: https://scholarsmine.mst.edu/cgi/viewcontent.cgi?article=1051&context=inspire-meetings#:~:text=The%20robot%20utilizing%20adhesion%20force,transferring%20points%20and%20overcome%20obstacles.

[38] S. T. Nguyen and H. M. La, "Development of a steel bridge climbing robot," in *2019 IEEE/RSJ International Conference on Intelligent Robots and Systems (IROS)*, 2019, pp. 1912–1917.

[39] "U.S Department of Transportation Highway Administration, National Bridge Inventory Data, 2019," http://www.fhwa.dot.gov/bridge/nbi.cfm.

[40] ASCE, "2017 infrastructure report card," https://www.infrastructurereportcard.org/wp-content/uploads/2017/01/Bridges-Final.pdf, 2017.

[41] N. T. S. Board, "Highway accident report, collapse of i-35w highway bridge," 2008. [Online]. Available: https://web.archive.org/web/20130622105807/http://www.ntsb.gov/investigations/summary/HAR0803.htm

[42] M. Caputo, "The economic cost of the bridge collapse," 2007. [Online]. Available: https://www.mprnews.org/story/2007/08/02/commercecosts

[43] S. T. Nguyen, A. Q. Pham, C. Motley, and H. M. La, "A practical climbing robot for steel bridge inspection," in *2020 IEEE International Conference on Robotics and Automation (ICRA)*, 2020, pp. 9322–9328.

[44] M. Eich and T. Vögele, "Design and control of a lightweight magnetic climbing robot for vessel inspection," in *the 19th Mediterranean Conf. on Control Automation*, June 2011, pp. 1200–1205.

[45] S. Buckley, "Japanese bridge inspection robot has magnetic wheels, shuffles up walls," 2013. [Online]. Available: https://www.engadget.com/2013-12-21-birem-robot-has-magnetic-wheels.html

[46] Helical-Robotics, "Climbing robots for wind turbine inspection," 2013. [Online]. Available: https://inhabitat.com/helical-robotics-introduces-climbing-robots-for-wind-turbine-inspection/

[47] P. J. Blau, *Friction Coefficient.* Boston, MA: Springer US, 2013, pp. 1304–1306. [Online]. Available: https://doi.org/10.1007/978-0-387-92897-5_169

[48] A. Bauchau, "Euler-bernoulli beam theory," in *Structural Analysis*, 2009.

[49] W. D. C. Jr. and D. G. Rethwisch, *Materials Science and Engineering: An Introduction, 10th Edition.* Wiley, 2018.

[50] R. C. Hibbeler, *Engineering Mechanics, Statics.* Pearson, 2016.

[51] C. Ross, J. Bird, and A. Little, *Mechanics of Solids, 2th Edition.* B/W Illustrations, 2016.

[52] AZoM, "Aisi 1018 mild/low carbon steel, mechanical properties," 2012. [Online]. Available: https://www.azom.com/article.aspx?ArticleID=6115

[53] AZOMaterials, "Emulsion polymerised styrene butadiene rubber (e-sbr) – mechanical, electrical and cure properties and resistance to fluids," 2003. [Online]. Available: https://www.azom.com/article.aspx?ArticleID=1844,https://www.azom.com/properties.aspx?ArticleID=1844

[54] P. Mitiguy, *Advanced Dynamics and Motion Simulation.* Motion Genesis, LLC, 2021.

[55] I. N. R. Siegwart, EPFL, *Introduction to Autonomous Mobile Roboitcs.* MIT Press, 2011.

[56] J. L. Meriam, L. G. Kraige, and J. N. Bolton, *Engineering Mechanics: Dynamics, 9th Edition.* Wiley, 2018.

[57] H. D. Bui, S. Nguyen, U. H. Billah, C. Le, A. Tavakkoli, and H. M. La, "Control framework for a hybrid-steel bridge inspection robot," in *2020 IEEE/RSJ International Conference on Intelligent Robots and Systems (IROS)*, 2020, pp. 2585–2591.

[58] H.-D. Bui and H. M. La, "Navigation framework for a hybrid steel bridge inspection robot," in *arXiv, cs.RO, 2101.02282*, 2021.

[59] D. Bui and H. M. La, "Control and navigation framework for a hybrid steel bridge inspection robot," in *arXiv, cs.RO, 2102.00641*, 2021.

[60] C. Motley, S. T. Nguyen, and H. M. La, "Design of a high strength multi-steering climbing robot for steel bridge inspection," *2021 International Conference on Intelligent Robots and Systems (IROS)*, 2021. [Online]. Available: https://www.overleaf.com/project/6008c92bc58c5c6c2e1c92df

[61] A. Q. Pham, C. Motley, S. T. Nguyen, and H. M. La, "A robust and reliable climbing robot for steel structure inspection," *Under review*, 2021.